行政院國家科學委員會專題研究計畫成果報告

極化載波重複使用之通信系統結案報告

Polarized Carriers Reuse Communication System

計劃編號:NSC89-2213-E-002-061

NSC89-2213-E-002-199

NSC90-2213-E-002-041

執行期限: 88 年 8 月 1 日至 91 年 7 月 31 日

主持人: 吳靜雄教授, 台灣大學教授

參與人員: 楊順安、吳孟哲、周子涵、孫偉男、魏南榕、陳建全、張嘉宜

因會出席國際會議心得報告

1. 中文摘要

本計畫主要研究偏極化電波在無線通訊系統之研究,並且延伸至多維天線傳輸之通訊系統。當存在直接波(Line of Sight)時,利用相互垂直的偏極化電波可以使用相同的頻道傳送兩倍的資料量. 即使在多路徑衰減的通道上,由於不同偏極化電波所經不同的傳播路徑不相同造成互相獨立的多路徑衰減,配合適當的傳送信號設計,亦能使系統的容量(capacity)增加. 本計畫總共執行三年, 執行期間主要研究方向包含多維天線偏極化傳輸技術及通訊系統,雙偏極化頻率重複使用及頻率配置方式, 多重輸入輸出(MIMO)正交頻譜多工(OFDM)系統. 多輸入多輸出(MIMO)無線通信系統中通道估測問題，最佳化的指引符碼(pilot symbol)所應滿足條件以及構建方式。都卜勒效應下的多重輸入輸出通訊系統的同步研究. 時空編碼在多維天線系統中的應用等.

關鍵詞：極化調變，極化載波重複使用，極化，無線通信

2. Abstract

The main object of this research is to use polarized waves that carry independent information to increase the spectrum efficiency. The research activity is further extended to multiple antenna system since many of the problems are quite similar. The main research results include "Dual-Polarization Frequency Reuse with Frequency Band Shifting Allocation"[1], "A New Dual Polarization Wave

Reuse Communication System for Cross Polarization and Antenna Misalignment Channel"[10,11], "A NEW PER TONE EQUALIZATION STRUCTURE FOR MIMO OFDM SYSTEM"[4], "Optimal Binary Training Sequence Design for Multiple-Antenna Systems over Dispersive Fading Channels" [5], "A Robust Timing Synchronization Scheme in Multiple Antenna Systems with Doppler Frequency Shifts" [6], "Performance Analysis of 16 QAM OFDM Transmission with Polarization Diversity Over Dispersive Fading Channel" [7], "MC-MLSE of Space-Time Coded Signals over Dispersive Channels" [8], etc.

KEY WORDS
MIMO, Timing Synchronization, Pilot Symbols, Doppler Spread, OFDM, polarization, multiple antenna, diversity,

3、Research Results

3.1 Dual-Polarization Frequency Reuse with Frequency Band Shifting Allocation

In wireless communications, spectrum is one of the most important resources. To increase spectrum utilization efficiency, many schemes, such as Orthogonal Frequency Division Multiplexing (OFDM) [9-11], cellular frequency reuse, and dual-polarization frequency reuse [12, 13], were proposed and deployed. OFDM is an attractive technique for digital transmission. Spectrum utilization efficiency can be increased by the orthogonal frequency spacing and signal bands overlapping. But the effects of frequency offset, multipath fading, and delay deeply effect the effectiveness of OFDM. The dual polarization frequency reuse system, which uses orthogonally polarized electromagnetic (EM) waves, has been demonstrated in satellite communications. The linear and circular types of polarization are the most frequently used. There are two directions of polarization (DoPs), vertical and horizontal, in the linear-polarized system and two DoPs, clockwise and counterclockwise, in the circular-polarized system. In principle, transmission through orthogonal polarization carriers doubles the system capacity. But practically, it is hard to achieve because of propagation impairments and antenna imperfections. The propagation impairments, such as rainfall attenuation, depolarization, and cross polarization interference (CPI) deteriorate the signal transmission in the satellite-earth station links. Some compensation methods were reported in the literature [14-17]. Furthermore, the problems will become more complicated by the multipath fading effect when transmitting in the terrestrial environment. Although some schemes, such as equalization and diversity, are proposed to overcome the problems, they are too complicated to be practical. Therefore, we adopt the concept of orthogonal frequency spacing used in OFDM and apply to the linear dual-polarization system. The signal band allocation and orthogonal frequency spacing between the vertical and horizontal DoPs are introduced. Consequently, the performance degradation problem can be easily solved. The proposed system may employ pilot symbols for channel coefficients estimation, carrier recovery, etc.. Furthermore, band-edged pilot tones can be

added in the proposed system, which is impossible for a conventional OFDM system.

In the traditional dual-polarization frequency reuse system, the signal spectra of both DoPs completely overlap. Guard bands between signal spectra are needed to prevent adjacent channel interference due to the imperfection of bandpass filter. The difference between the proposed system and the traditional system is that the vertical polarization (ie. y DoP) signal spectra are located at the higher frequency band relative to the horizontal polarization (ie. x DoP) signal spectra by the amount of symbol rate, B, in the proposed system. The system architecture and behavior are described as next.

The schematic of the transmitter is shown in Fig. 3.1.1. The function of the serial-to-parallel converter (SPC) will be described later, and the system description begins with the two input data streams, $e_{ix}(t)$ and $e_{iy}(t)$, which are modulated by Modulator 1 (Mod.1) and Modulator 2 (Mod.2) respectively. Any modulation scheme can be adopted. In this section, the dual-QPSK scheme is considered. After modulation, the modulated symbols are fed into the square-rooted raised cosine band-limited (BL) filters and then transmitted through the x DoP and the y DoP antennas. To maintain orthogonality and to estimate channel parameters, the narrow-band pilot tones (PTs), which are produced by the PT generators with the band-edged frequency shifter (BEFS) are added. The spectra allocation of PTs are chosen at the edges of the spectra of the corresponding in-band signals as shown in Fig. 3.1.2(a). The number of pilot tones and their spacing interval depend on the channel complexity. Moreover, pilot signal can be designed to carry more information about the channel in order to get better channel estimation. After adding the filtered symbols and pilot tones, the system up-converts the x DoP signal and the y DoP signal to two frequency bands, f_{ix} and f_{iy}, respectively, where i denotes the ith signal channel. f_{ix} and f_{iy} differ by the amount of symbol rate, so the two signals are linearly independent theoretically. If the width of the guard band is less than the signal bandwidth, the spectra of x DoP signal in the ith channel and y DoP signal in the (i-1)th channel overlap because of the band allocation. The sketch of signal spectrum allocation is depicted in Fig. 3.1.2(b), which shows that the two different DoP signal spectra in adjacent channels are separated by the value of bit rate plus f_d. f_d can be considered as the width of guard band. Theoretically, if f_d equals zero, the two signals are orthogonally spaced with zero-interference. However, the value of f_d can be adjusted to control the frequency band allocation for the spectra of PTs. On the other hand, f_d is also prepared for compensating the Doppler effect. There is a limit that f_d can not be negative, i.e. overlapping the signal bands of the two adjacent channels in the same DoP is not allowed.

The schematic of the receiver is shown in Fig. 3.1.3. After down-converting the received signals, PT filtering and signal filtering are processed respectively. The pilot tones are filtered out by the PT filters and the signals are sent into the polarization recovery circuit and carrier recovery circuit, which we will not discuss further. The received symbols are filtered by the square-rooted raised cosine

band-limited filters. The merit of using the filter is that we can take the advantage of the properties of raised cosine filter without using other types of low pass filters. Then the filtered symbols are fed into the demodulators with the reference recovered from the pilot tones. The detected data streams, $\hat{e}_{ix}(t)$ and $\hat{e}_{iy}(t)$, are obtained. The function of the parallel-to-serial converter (PSC) will be described later.

The multipath Rayleigh-fading channel with Doppler effect [18, 19] is considered. Taking the inherent limitation of dual-polarization transmission into account, we only analyze the two-ray case. The impulse responses of the dual polarized channel are given by

$$h_x(t) = \alpha_x \delta(t) + \gamma_x A_x \delta(t-\tau_x) e^{j\varphi_x} e^{j2\pi f_D t},$$

$$for\ xDoP, \qquad (3.1.1)$$

and

$$h_y(t) = \alpha_y \delta(t) + \gamma_y A_y \delta(t-\tau_y) e^{j\varphi_y} e^{j2\pi f_D t}$$

$$for\ yDoP \qquad (3.1.2)$$

where α_j is the attenuation coefficient, $\delta(.)$ is the delta-function, f_D is the Doppler shift, τ_j is the delay time of the second path relative to the line-of-sight, γ_j is the square-rooted power ratio with respect to the first path, φ_j is the initial phase of the second path, A_j is a Rayleigh random variable with unity second moment, and j=x,y denotes the x DoP and y DoP. Because Doppler effect results from the relative velocity between transmitter and receiver, it is reasonable to set the same Doppler shift, f_D, in both x DoP and y DoP.

Pilot tones are conducive to the estimation of the channel parameters. There is at least one pilot tone in each coherent bandwidth. The theoretical functions of reflection coefficients of horizontal-polarized wave and vertical-polarized wave were discussed in the literature [18]. For horizontal polarization, the function indicates that the relative phase of the incident and reflected waves is nearly 180° for all angles of incidence. But for vertical polarization, the results are quite different. When the angle of incidence is small, the behaviors of horizontal and vertical polarization are almost the same. But as the angle of incidence increases, the magnitude and relative phase of the reflected wave decrease rapidly. It's a torment to recover the vertical polarization wave. However, with the existence of pilot tones in the system, this problem can be solved. Both reflection coefficients are frequency dependent. Therefore, the relative phase changes of both pilot tone and in-band signal are almost the same. We can recover the carrier phase by the pilot tones easily.

In the traditional dual-polarized systems, each DoP is used as an independent transmission channel. It means that the data streams transmitted in both DoPs are uncorrelated. For better transmission performance, the error correction code (e.g. convolutional code) can be used with expanding the code word by some redundant bits. And the training sequence which estimates the channel characteristic can also be used. To save the transmission payload, the concept of parallel transmission in OFDM [17] can be introduced to reduce the code redundancy. In Fig. 3.1.1, the coded data stream is fed into the SPC and split into two data sequences, $e_{ix}(t)$ and $e_{iy}(t)$. The

consequent processes were indicated in the previous sections. The receiving processes in the receiver are also illustrated in Fig. 3.1.3. Finally, the desired coded data stream is obtained by sending the detected data sequences, $\hat{e}_{ix}(t)$ and $\hat{e}_{iy}(t)$, through the PSC.

Here we consider the dual-QPSK system and express the input data sequence to the signal space in complex domain. The symbols of x DoP and y DoP in the kth duration are denoted by

$$u_{ix}(t-kT) = a_i(t-kT) + jb_i(t-kT) \quad (3.1.3)$$

$$u_{iy}(t-kT) = c_i(t-kT) + jd_i(t-kT) \quad (3.1.4)$$

where $a_i(t)$ and $c_i(t)$ are the QPSK signals in the I-branch of x and y DoPs in the ith channel, respectively. $b_i(t)$ and $d_i(t)$ are the QPSK signals in the Q-branch of both DoPs in the ith channel. Thereafter, a_k^i will represent $a_i(t\text{-}kT)$ for convenience. T denotes the symbol duration of the QPSK modulators. The outputs of the modulators are sampled every T seconds and then passed through the squared-root raised cosine filter with the impulse response p(t). After up converting the mapped signals to the carrier frequencies, we get the transmitting signals as

$$S_{ix}(t) = \sum_{k=-\infty}^{\infty} \sqrt{2} u_{ix}(t-kT) p(t-kT) \exp(j2\pi f_{ix} t) \quad (3.1.5)$$

$$S_{iy}(t) = \sum_{k=-\infty}^{\infty} \sqrt{2} u_{iy}(t-kT) p(t-kT) \exp(j2\pi f_{iy} t). \quad (3.1.6)$$

Because of the orthogonality between $S_{ix}(t)$ and $S_{iy}(t)$, they do not interfere with each other. However, $S_{ix}(t)$ will be interfered by the adjacent channel signals, $S_{(i-1)y}(t)$, and the delayed signal due to propagation imperfection. Similarly, $S_{iy}(t)$ will be interfered by $S_{(i+1)x}(t)$ and the delayed signal. Here we only present the x DoP case because the other is exactly the same.

At the receiver, the received signal of x DoP is given by

$$r_{ix}(t) = y_{ix}(t) + n_{ix}(t) \quad (3.1.7)$$

where $n_{ix}(t)$ is the additive white Gaussian random process with zero mean and the variance $N_0/2$. $y_{ix}(t)$ is the x DoP channel output with the inputs, $S_{ix}(t)$ and $S_{(i-1)y}(t)$. It can be expressed as

$$y_{ix}(t) = \mathrm{Re}\{\alpha_x(S_{ix}(t) + RS_{(i-1)y}(t)) + \beta_1[\gamma_x A_x S_{ix} \cdot (t-\tau_x)e^{j\varphi_x} + R\gamma_y A_y S_{(i-1)y}(t-\tau_y)e^{j\varphi_y}]e^{j2\pi f_D t}\} \quad (3.1.8)$$

The first term is the line-of-sight signal. The second term is the delayed signal and interference with delay time τ_x and τ_y of x and y DoPs', respectively. α_x is the attenuation coefficient. The coefficient, R, is the cross-polarization coefficient, satisfying $0 \le R \le 1$. β_1 is the polarization-mismatch coefficient of delayed symbol of the second path. It lies between 0 and 1. The frequency f_D is the Doppler shift in the second path. In the following analysis, we will take values all normalized to α_x, i.e $\alpha_x=1$.

At the BL filter output, we get the sampled signal, Z_{ix}. Then we analyze two different cases: the mutually dependent Rayleigh fading channel and independent Rayleigh fading channel. The BER performance is influenced by several factors.

a. power strength of the second path

The influence of the square-root power ratio of the first and the second paths, γ, and the correlation between the polarizations of line-of-sight and the second path, β_1, is shown

in Fig. 3.1.4. When γ increases from 0.15 to 0.25 at β_1=0.95, the system performance is degraded about 2 dB at the BER of 10^{-4}. And for fixed γ=0.2, the performance degrades about 1.5 dB when β_1 increases from 0.35 to 0.95. It implies that the performance is sensitive to the power strength of the second path signal. Because of the delay of the second path, the effect of ISI has to be considered. In general, the averaged BER is dominant by the worst case. Therefore, the performance will be better with smaller β_1, i.e. the lower polarization correlation between the line-of-sight signal and the second path signal yields better performance.

b. effect of cross-polarization interference(CPI)

The performance for various values of the CPI coefficient, R, is shown in Fig. 3.1.5. It indicates that CPI does not impact the performance at all. The reason is that the orthogonal frequency shifting has eliminated the damage of cross-polarization interference. This is the merit of the system, and we can save the effort to compensate cross-polarization problems. The anti-CPI characteristic can be observed more clearly in Fig. 3.1.6. When $\delta \geq 0$ (i.e. frequency shift is larger than the orthogonal frequency), the BER is constant no matter what the value of R is. When δ=-0.3 (i.e. frequency shift is smaller than the orthogonal frequency), the performance is getting worse with larger R. Furthermore, comparison of the two delay times of x and y DoPs is shown in Fig. 3.1.7, where $\Delta_1=\tau_x/T$ and $\Delta_2=\tau_y/T$ are the normalized delay times with respect to the symbol duration. It shows that the performance is significantly impacted by the values of the parameter Δ_1 but is not influenced by the values of Δ_2. Therefore, the delay interference produced by the second path signal of the other DoP can be completely ignored.

c. guard band

Because of the existence of guard band (as shown in Fig. 3.1.2), the spectrum of $S_{ix}(t)$ is not orthogonally allocated with $S_{(i-1)y}(t)$ (i.e. the normalized shifting frequency, δ, has to be larger than zero). Fig. 3.1.8 illustrates the relation between the BER and δ. It shows that the BER is almost constant when δ is larger than zero. So, the system performance does not change when the guard band exists.

d. effect of Doppler shift

The relation between the BER and the roll-off factor, β, is shown in Fig. 3.1.9. The BER for Δ=0.2 has a peak when β is about 0.2. Similarly, for Δ=0.3, the BER has a peak when β is about 0.3. It implies that the BER is degraded significantly when β and Δ have about the same value. This phenomenon is caused by the Doppler shift. Generally speaking, slight frequency shift caused by the channel impairments will dominate the system performance. When slight frequency shift occurs, it has huge interference. Moreover, there is a second peak around β=0.8 in Fig. 3.1.9. It's important to estimate the most probable f_D and to choose appropriate value of β to avoid BER degradation.

e. performance comparison

Comparison with other systems is shown in Fig. 3.1.10. The performances of the proposed, conventional OFDM and dual-polarization canceler with bootstrap [20] systems are

presented. The performance improvement of the proposed system over the dual-polarization canceler with bootstrap system is about three orders of magnitude at E_b/N_0=14 dB. The performance improvement over the conventional OFDM system is about three and half orders of magnitude at the same value of E_b/N_0. It is believed that the proposed system outperforms the other.

3.2 A New Dual Polarization Wave Reuse Communication System for Cross Polarization and Antenna Misalignment Channel

Dual polarization systems exploit the orthogonality of polarized waves so that signals can be transmitted through each polarization. The channel capacity can be doubled if the channel state is ideal. These systems operate mainly in the line of sight (LOS) environments such as satellite communications or some fixed wireless communications [12,22,23,24]. However, they may suffer from cross depolarization coupling, for example, caused by heavy rain [12]. In addition, antennas alignment is important to mitigate the effect of mutual interference [24]. Nevertheless, mobility is a desirable feature for a lot of wireless communication systems. Random locations and orientations of the receiver antennas may cause problem for these systems designed to operate in the LOS environment.

In the literature, systems using completely different schemes of multiple antenna systems are reported to exploit independence of the channel fading in each transmit-receive antenna pair [25-28]. In these systems, the antennas should be properly separated or using different polarizations and the transmission channel is full of multipath scatterings to achieve independence of fading. The channel capacity increases approximately proportionally to the number of antennas theoretically. Various types of space-time codes have been proposed to get the diversity and coding gains simultaneously [26,29].

However, for many wireless communications applications, the transmission channel is time-varying and depends on the operating environment. Sometimes we have LOS path and sometimes we don't. In this section, we propose a multiple antenna system that performs well in both LOS and multipath rich environments. We use three mutually orthogonal antennas in the transmitter and the receiver so that the system is robust to random orientation in the LOS environment. In addition, we also apply space-time codes to protect the data so that the system performs well in non-line of sight (NLOS) environments. Two different categories of space-time codes are employed to investigate the system performance both in LOS and NLOS environments. One is based on the Euclidean distance criterion (EDC) and the other is based on rank and determinant criterion (RDC) [29]. Two different constellation mappings are investigated. One transmits equal power from each antenna and the other transmits orthogonal eigen-signals by using feedback channel information. We study the robustness of this scheme with feedback information error. Moreover, we also compare the performances of the proposed communication system to another

one with three collinear antennas. The results show that the proposed system maintains satisfactory performance but that of the collinear antenna set deteriorates seriously due to random orientation in the LOS environments.

The block diagram of the transmitter is depicted in Fig. 3.2.1 (a). The binary data are fed into the series to parallel converter and then input to the space-time (ST) encoder. The ST encoder generates the coded symbol vectors, which are mapped into the corresponding baseband signals. These signals are up-converted to the carrier frequency and transmitted from the antenna set. Orthogonal pilot symbols are embedded at the beginning of each transmitted frame. The transmitter employs three orthogonal antennas such that it is robust to random relative direction of the transmitter and the receiver antennas.

The receiver block diagram is shown in Fig. 3.2.1 (b). We assume that the orientations of the three mutually orthogonal receiver antennas do not have to be aligned with the transmitter antennas but are uniformly distributed in all directions. The channel estimator obtains the estimated channel matrix from the received pilot signals. Then, the Viterbi decoder computes the trellis transition diagram according to the transmitted constellation and the estimated channel matrix. The receiver may feedback the channel matrix or the suggested constellation through the feedback channel to the transmitter if the channel matrix varies slowly.

In Fig. 3.2.2(a), we illustrate the relative location and orientation of the 3-dimensional antenna sets of the transmitter and the receiver, which consist three orthogonal short dipole antennas. The transmitter antennas are denoted by Tx, Ty, and Tz. The aligned receiver antennas are represented by Rxa, Rya, and Rza, and the receiver antennas with random orientations are denoted by Rx, Ry and Rz. Assuming that the transmitter is located at the origin of the coordinates with Tx, Ty, and Tz oriented in the x, y, and z axes and the receiver is located at the spherical coordinates (r,θ,ϕ). The orientations of the receiving antennas, (Rx,Ry,Rz), are represented by the Euler's angles, (α,β,γ) in reference to (Rxa, Rya, Rza), which are obtained as follows: first, we fix Rza, and rotate Rxa and Rya by α radian. Next, fix Rxa, and rotate Rya and Rza by β radian. Finally, fix Rza again and rotate Rxa and Rya by γ radian. Assuming that the location and orientation of the receiver are uniformly distributed over all directions in the space, the probability density functions of the above parameters are given by

$$f_\theta(\theta)=\frac{1}{2}\sin(\theta), \qquad \theta\in[0,\pi], \quad (3.2.1)$$

$$f_\phi(\phi)=\frac{1}{2\pi}, \qquad \phi\in[0,2\pi), \quad (3.2.2)$$

$$f_\alpha(\alpha)=\frac{1}{2\pi}, \qquad \alpha\in[0,2\pi), \quad (3.2.3)$$

$$f_\beta(\beta)=\frac{1}{2}\sin(\beta), \qquad \beta\in[0,\pi], \quad (3.2.4)$$

and $$f_\gamma(\gamma)=\frac{1}{2\pi}, \qquad \gamma\in[0,2\pi). \quad (3.2.5)$$

Short dipole antennas, with length ℓ much smaller than the carrier wavelength λ, are employed. Thus, the far field induced by Tz is given by [30]

$$E_\theta = j\frac{I\ell}{2\lambda}\left(\frac{e^{-j2\pi r/\lambda}}{r}\right)\eta_0\sin(\theta)\hat{\theta}, \quad (3.2.6)$$

where η_0 is the intrinsic impedance of the free

space, I is the current on the dipole, and $\hat{\theta}$ denotes the unit vector of the spherical coordinate.

The transmitted signal is expressed as

$$\vec{S}(t) = \sum_{k=1}^{L} \mathrm{Re}\{[s_1(k)\vec{i}_t + s_2(k)\vec{j}_t + s_3(k)\vec{k}_t]\mathrm{p}(t - kT_s)e^{jwt}\}\ , \tag{3.2.7}$$

where T_s is the symbol duration and w is the radian frequency of the carrier. $\vec{i}_t$, $\vec{j}_t$ and $\vec{k}_t$ denote the directions of the three transmitting antennas, respectively, $s_1(k)$, $s_2(k)$ and $s_3(k)$ are complex valued variables representing the transmitted signals and $p(t)$ is the pulse shaping function. Assuming flat multipath fading channel, we can express the received signal as follows.

$$\vec{R}(t) = \sum_{k=1}^{L} \mathrm{Re}\{[r_1(k)\vec{i}_r + r_2(k)\vec{j}_r + r_3(k)\vec{k}_r]\mathrm{p}(t - kT_s)e^{jwt}\}\ , \tag{3.2.8}$$

where $\vec{i}_r, \vec{j}_r$ and $\vec{k}_r$ denote the directions of the three receiving antennas. $r_1(k)$, $r_2(k)$ and $r_3(k)$ are complex valued variables representing the received signals.

We can express the received signals in terms of the channel matrix, the transmitting signals and noise as follows.

$$\mathbf{r}(k) = \mathbf{H}\mathbf{s}(k) + \mathbf{n}(k) \tag{3.2.9}$$

where

$$\mathbf{r}(k) = [r_1(k)\ r_2(k)\ r_3(k)]^T, \tag{3.2.10}$$

$$\mathbf{H} = \begin{bmatrix} h_{11} & h_{12} & h_{13} \\ h_{21} & h_{22} & h_{23} \\ h_{31} & h_{32} & h_{33} \end{bmatrix}, \tag{3.2.11}$$

$$\mathbf{s}(k) = [s_1(k)\ s_2(k)\ s_3(k)]^T \tag{3.2.12}$$

and $\mathbf{n}(k) = [n_1(\mathrm{k})\ n_2(\mathrm{k})\ n_3(k)]^T$. (3.2.13)

The entries of $\mathbf{n}(k)$ are modeled as independent zero mean complex Gaussian variables with variance σ_n^2. We assume that the propagation channel includes a line of sight path and multipath scattering components. The expected power of the LOS component is K_r -fold that of the multipath components. Thus, $\mathbf{H}$ is expressed as

$$\mathbf{H} = \sqrt{\frac{K_r}{1+K_r}}\mathbf{H}_{LOS} + \sqrt{\frac{1}{1+K_r}}\mathbf{H}_{NLOS}, \tag{3.2.14}$$

where $\mathbf{H}_{LOS}$ and $\mathbf{H}_{NLOS}$ denote the normalized line of sight component and the multiple path component, respectively. The elements of $\mathbf{H}_{LOS}$ and $\mathbf{H}_{NLOS}$ are normalized to have unity variance. Based on (3.2.6), $\mathbf{H}_{LOS}$ can be obtained as

$$\mathbf{H}_{LOS} = \mathbf{H}_R\mathbf{H}_{LOS,A}, \tag{3.2.15}$$

where $\mathbf{H}_{LOS,A}$ is the channel matrix with the aligned antenna set (Rxa, Rya, Rza) given by

$$\mathbf{H}_{LOS,A} = \sqrt{\frac{9}{2}}\begin{bmatrix} \sin^2(\theta)\sin^2(\phi)+\cos^2(\theta) & -\sin^2(\theta)\sin(\phi)\cos(\phi) & -\sin(\theta)\cos(\theta)\cos(\phi) \\ -\sin^2(\theta)\sin(\phi)\cos(\phi) & \cos^2(\theta)+\sin^2(\theta)\cos^2(\phi) & -\sin(\theta)\sin(\phi)\cos(\theta) \\ -\sin(\theta)\cos(\phi)\cos(\theta) & -\sin(\theta)\sin(\phi)\cos(\theta) & \sin^2(\theta) \end{bmatrix} \tag{3.2.16}$$

and $\mathbf{H}_R$ is obtained through multiplication of the three matrice representing rotations described by the Euler's angles. $\mathbf{H}_R$ is given by

$$\mathbf{H}_R = \mathbf{H}_\gamma\mathbf{H}_\beta\mathbf{H}_\alpha, \tag{3.2.17}$$

where

$$\mathbf{H}_{\alpha}=\begin{bmatrix}\cos\alpha & \sin\alpha & 0\\ -\sin\alpha & \cos\alpha & 0\\ 0 & 0 & 1\end{bmatrix}, \qquad (3.2.18)$$

$$\mathbf{H}_{\beta}=\begin{bmatrix}1 & 0 & 0\\ 0 & \cos\beta & \sin\beta\\ 0 & -\sin\beta & \cos\beta\end{bmatrix}, \qquad (3.2.19)$$

and $$\mathbf{H}_{\gamma}=\begin{bmatrix}\cos\gamma & \sin\gamma & 0\\ -\sin\gamma & \cos\gamma & 0\\ 0 & 0 & 1\end{bmatrix}. \qquad (3.2.20)$$

For the multipath component, we assume that the transmitting direction and the receiving direction are all uniformly distributed. When the number of paths is large, the channel gain taps can be modeled by Rayleigh fading channel. Thus, the entries of $\mathbf{H}_{NLOS}$, $h_{mn,NLOS}$,are independent complex Gaussian random variables with zero mean and variance one.

For comparison, we also derive the channel model for the communication systems using three collinear antenna sets with the same polarization. The relative location and orientation of the antenna sets are depicted in Fig. 3.2.2(b). The transmitting antennas are denoted by T1, T2, and T3, the aligned receiving antennas are represented by R1a, R2a, and R3a and the randomly oriented receiving antennas are denoted by R1, R2, and R3. We assume that the center of T2 is located at the origin of the coordinate with the dipole antenna oriented in the z direction. The separation of the adjacent antennas in the antenna sets is denoted by d .

Two different constellations are considered.

a. Without feedback information

When the channel is time-variant or the CSI is not available, we just transmit equal energy signals from all antennas. Thus, we have three complex variables, $[s_1(k)\ s_2(k)\ s_3(k)]^T$, to carry information. The transmission constellations are shown in Fig. 3.2.3 with A equal to $\sqrt{E_s/6}$ for all $s_m(k)$, $m=1\sim 3$. Where E_s represents the total energy transmitted from the three antennas in a symbol duration.

b . With feedback information

For perfect LOS channels, i.e. $K_r=\infty$, we have $\mathbf{H}=\mathbf{H}_{LOS}$. Thus, the eigenvalues of $\mathbf{H}^H\mathbf{H}$ are $\frac{9}{2},\frac{9}{2}$, and 0, and the corresponding eigenvectors are

$$\psi_{1,LOS}=\begin{bmatrix}0\\ -\cos(\theta)\\ \sin(\theta)\sin(\phi)\end{bmatrix}, \qquad (3.2.21)$$

$$\psi_{2,LOS}=\begin{bmatrix}\cos(\theta)\\ 0\\ -\sin(\theta)\cos(\phi)\end{bmatrix}, \qquad (3.2.22)$$

$$\psi_{3,LOS}=\begin{bmatrix}\sin(\theta)\cos(\phi)\\ \sin(\theta)\sin(\phi)\\ \cos(\theta)\end{bmatrix}. \qquad (3.2.23)$$

We observe that the two larger eigenvalues are the same and the third one is 0. Thus, we can expect that there are two large eigenvalues and a small one when K_r is large. For convenience, let's denote the eigenvalues by λ_1, λ_2 and λ_3 in descending order. The corresponding unitary eigenvectors are represented by ψ_1, ψ_2, and

ψ_3. In Fig. 3.2.4, we show the cumulative distributions of the relative magnitudes of the eigenvalues, i.e. λ_2/λ_1 and λ_3/λ_1. We can see that, when K_r is greater than 5, the probability that λ_2/λ_1>0.3 is greater than 0.9. However, the third eigenvalue is quite small for most of the time and it is not efficient to transmit the signal power via the eigenvector with small eigenvalue. This motivates us to use only two eigenvectors with the larger eigenvalues to transmit signals.

The constellation is determined as follows. First, the receiver obtains the estimate of channel matrix, $\mathbf{H}$, and calculates the eigenvectors and the corresponding eigenvalues of $\mathbf{H}^H\mathbf{H}$. According to the channel information, the transmitter determines the transmitted symbols as

$$\mathbf{S}_m = w_{m1}\psi_1 + w_{m2}\psi_2, \qquad (3.2.24)$$

and the symbols are mapped to the values of w_{m1} and w_{m2}.

Two different methods of designing the values of w_{m1} and w_{m2} are investigated. The first one is to transmit equal energy (E-T) via w_{m1} and w_{m2}, i.e. $|w_{m1}|=|w_{m2}|$. The other one is to transmit different energy via w_{m1} and w_{m2} such that the received signals $w_{m1}\mathbf{H}\psi_1$ and $w_{m2}\mathbf{H}\psi_2$ have the equal energy (E-R). Note that $w_{m1}\mathbf{H}\psi_1$ and $w_{m2}\mathbf{H}\psi_2$ are orthogonal since

$$(w_{m1}\mathbf{H}\psi_1)^H w_{m2}\mathbf{H}\psi_2 = w_{m1}^* w_{m2}\psi_1^H\mathbf{H}^H\mathbf{H}\psi_2 = 0. \qquad (3.2.25)$$

In addition, the received energy is given by

$$(w_{m1}\mathbf{H}\psi_1)^H w_{m1}\mathbf{H}\psi_1 = \lambda_1|w_{m1}|^2 \qquad (3.2.26)$$

and $$(w_{m2}\mathbf{H}\psi_2)^H w_{m2}\mathbf{H}\psi_2 = \lambda_2|w_{m2}|^2 \qquad (3.2.27)$$

Thus, we have

$$\lambda_1|w_{m1}|^2 = \lambda_2|w_{m2}|^2. \qquad (3.2.28)$$

The symbol constellations of w_{m1} and w_{m2} are the same as Fig. 3.2.3. For E-T constellation, the amplitude A equals $\sqrt{E_s/4}$, which is the same for w_{m1} and w_{m2}. For the E-R constellation, the amplitude, A, equals $\sqrt{\lambda_1 E_s/2(\lambda_1+\lambda_2)}$ for w_{m1} and $\sqrt{\lambda_2 E_s/2(\lambda_1+\lambda_2)}$ for w_{m2}, respectively.

The numerical results of bit error probability are shown in Fig. 3.2.5, in which we normalize $\lambda_1 = 1$ and set $\lambda_2 = \lambda_{N,2}$. The result shows that E-R constellation outperforms the E-T constellation. Thus, we will apply E-R constellation in the following section.

The space-time codes proposed in [29] are applied in this communication system. In Fig. 3.2.6, we depict the structure of the encoder. Independent binary inputs, $I_1(k)$ and $I_2(k)$, belonging to $\{0,1\}$, are fed to the encoder. These binary inputs and the contents of the registers, $\mathrm{Reg}_{m,\upsilon}$, are multiplied by vectors $\mathbf{a}_{m,\upsilon}$, $m = 1,2$, $\upsilon = 1,2$, and then summed up, with mod 4 addition, to obtain the encoded symbol vector, $\mathbf{C}(k)$ as

$$\mathbf{C}(k) = \sum_{m=1}^{2}\left[I_m(k)\mathbf{a}_{m,0} + \sum_{\upsilon=1}^{2}\mathrm{Re}[g_{m,\upsilon}\mathbf{a}_{m,\upsilon}]\right] \bmod 4. \qquad (3.2.29)$$

Since there are four binary registers in this encoder, the number of states is 16. Two different categories of space-time codes are applied in this system. The first category is

based on Euclidean distance criterion (EDC) and the other is based on the rank and determinant criterion (RDC). The values of $\mathbf{a}_{m,v}$ are listed in Table 3.2.1, where n_T is the number of transmitting antennas. Orthogonal pilot symbols are transmitted from each antenna simultaneously in the header of each data frame. Assuming that the length of each training sequence is L_t, we denote the transmitted symbols from each antenna as $p_1(k)$, $p_2(k)$ and $p_3(k)$, $k = 1 \sim L_t$. The pilot sequences are mutually orthogonal. In other words, we have

$$\sum_{k=1}^{L_t} p_m(k) p_n^*(k) = 0 \quad \text{for } m \neq n, \quad (3.2.30)$$

where * denotes complex conjugate. The channel response is estimated by

$$\hat{x}_{mn} = \sum_{k=1}^{L_t} r_m(k) p_n^*(k) / \sum_{k=1}^{L_t} p_n(k) p_n^*(k), \quad (3.2.31)$$

where $r_1(k), r_2(k)$ and $r_3(k)$, $k = 1 \sim L_t$ are the received symbols.

We compare the outage performance of the systems with different antenna sets and different constellation design.

The channel capacity of the MIMO system is given by [31],

$$C = \log_2 \det[\mathbf{I}_{n_R} + \frac{SNR}{n_T} \mathbf{H}\mathbf{H}^*] \text{ bits/s/Hz.} \quad (3.2.32)$$

where n_R is the number of receiving antennas and $\mathbf{I}_{n_R}$ is an identity matrix of order n_R. The outage probability is defined by the probability that a given channel response has less capacity than the data information input to the channel. Given the channel matrix derived in Section III, we compute the outage probabilities for the communication systems with 3-D antenna sets and that with 3-L collinear antenna sets as shown in Fig. 3.2.7 where the data rate is 2 bits/s/Hz. For the collinear antenna set, the distance between transmitter and receiver is 50λ and the separation, d, between antennas is 0.5λ or 3λ. We denote the orthogonal antenna set by 3D. An interesting result is observed that the outage probability decreases with large K_r for the system with orthogonal antenna set while it decreases for that with the collinear antenna set. Because when K_r is large, the LOS component is the dominant path. Thus, the 3D antenna set still has two polarizations to transmit signal while for the 3L antenna set has only one polarization. In addition, the 3L antenna set suffers from random orientation.

In Fig. 3.2.8, we compare the performances with the two different type of space- time code in the 3-D antenna system. According to [29], EDC type space-time codes outperform the RDC type space-time codes at $K_r = 0$. Our result confirms that in [29]. Moreover, we find that the EDC type space-time codes outperform the RDC type for all values of K_r for both $n_T = 2$ and $n_T = 3$ in this channel model. The 'CSI' in the legend denotes the adaptive constellation with CSI where $n_T = 2$ is used. From Fig. 3.2.8, we find that the feedback constellation scheme outperforms the equal-constellation scheme when K_r is large. However, the improvement is not significant when the LOS component is small. In addition, we also investigate the effect of inaccurate feedback CSI. As a result of estimation error and channel variations, the feedback channel matrix, $\mathbf{X}_f$, may be different from the actual channel $\mathbf{X}_c$. Thus, we assume

that

$$\mathbf{X}_t = \mathbf{X}_c + \mathbf{X}_{T,E}, \qquad (3.2.33)$$

where the elements of $\mathbf{X}_{T,E}$ are assumed to be independent complex Gaussian random variables with zero means and identical variances $\sigma_{T,E}^2$. In Fig. 3.2.8, we also plot the system performance with $\sigma_{T,E}^2$=0.1. Space-time codes of EDC type are applied in the case. The results show that the degradation due to inaccurate feedback information is graceful.

In Fig. 3.2.9, we compare the performances of the system with 3-D antenna set to that with the collinear antenna set (3L). The Space-time code of EDC type with $n_T = 3$ is applied. We use the symbol constellation without feedback information as described previously. It is observed that the performance of the system with 3-D antenna set improves for large value of K_r while the performance of the system with 3-L antenna set deteriorates seriously.

In Fig. 3.2.10, we show the performance degradation of the systems due to imperfect channel estimation for the two different constellations, respectively. We assume that the variance of the estimation error, σ_E^2, for each element of the channel matrix is 0.01 and 0.1 in the simulations. We observe that the degradation is insignificant for error variance of 0.01.

In summary, we have proposed a new wireless communication system using three dimensional orthogonal antennas. Two different schemes are studied depending on the variation speed of the communication channel. The results show that the proposed system performs quite well with random orientations for both LOS and NLOS environments. We also investigate the performance of the similar system using collinear antenna sets. The result shows that the performance of the collinear antenna sets relies much on the correlation of the channel fading. In many applications, the appearance of LOS path may vary from time to time. Thus, the proposed system is suitable for applications such as wireless LAN or low power wireless communications.

3.3 A NEW PER TONE EQUALIZATION STRUCTURE FOR MIMO OFDM SYSTEM

MIMO transmission with inter-symbol interference (ISI) arises in many applications, such as multiuser communications, dual polarization radio transmission, and multisensor radar/sonar systems. Especially, the space-time coding system has demonstrated that system capacity can be significant increased and the performance is improved [25], MIMO related topics are developed zealously. Decision feedback equalization (DFE) structure and blind method are reported in the literature [32-36]. Recently, the optimal training sequence design in least square (LS) channel estimation is proposed [5].

On the other hand, OFDM is widely developed and used in wireless communication systems. Fig. 3.3.1 shows the general OFDM system block. OFDM can effectively utilize spectrum which is based on discrete Fourier transform (DFT) to provide orthogonal subcarriers with overlapping signal spectrum. By adding cyclic extended guard interval, OFDM has ability to mitigate the inter-symbol interference.

Here, we consider the MIMO OFDM system with per tone equalization over frequency selective fading channel. The channel effect on guarded OFDM signals is analyzed and the equalization schemes are presented. Furthermore, the system performance is analytically derived. The results show that the performance of this system is satisfactory under severe multipath environment.

In a single-input/single-output (SISO) system, the OFDM signal with cyclic extended guard interval transmitting over a frequency selective channel is considered as that the conventional OFDM signal (i.e. without guard interval) circularly convolves with the channel impulse response function. The channel output can be written as

$$y[k] = x[k] \otimes h[k] + n[k], \tag{3.3.1}$$

where $x[k]$ and $n[k]$ are conventional OFDM signal and additive white Gaussian noise, respectively, $h[k]$ is the channel impulse response function with finite length $\nu+1$ and $\otimes$ denotes the circular convolution operation. For the OFDM signal with N subcarriers, Equation (3.3.1) can be expressed in a matrix form as

$$\mathbf{y}_T = \mathbf{H}_T \mathbf{x}_T + \mathbf{n}_T , \tag{3.3.2}$$

where

$$\mathbf{x}_T = [x[N-1] \;\; x[N-2] \;\; \ldots \;\; x[0]]^T, \tag{3.3.3}$$

$$\mathbf{y}_T = [y[N-1] \;\; y[N-2] \;\; \ldots \;\; y[0]]^T, \tag{3.3.4}$$

$$\mathbf{n}_T = [n[N-1] \;\; n[N-2] \;\; \ldots \;\; n[0]]^T, \tag{3.3.5}$$

$$\mathbf{H}_T = \begin{bmatrix} h[0] & 0 & \cdots & 0 & h[\nu] & h[\nu-1] & \cdots & h[1] \\ h[1] & h[0] & \cdots & 0 & 0 & h[\nu] & \cdots & h[2] \\ \vdots & \vdots & \cdots & \vdots & \vdots & \vdots & \vdots & \vdots \\ 0 & \cdots & 0 & h[\nu] & h[\nu-1] & \cdots & h[1] & h[0] \end{bmatrix}. \tag{3.3.6}$$

Subscript T denotes the data in time domain, and superscript T is matrix transpose operation. Note that $\mathbf{H}_T$ is a circulant matrix with dimension $N \times N$ and the discrete Fourier basis is its eigenvector [37]. We can decompose matrix $\mathbf{H}_T$ and the frequency domain representation of $\mathbf{H}_T\mathbf{x}_T$ can be partitioned into two parts as

$$\mathbf{H}_T = \mathbf{F}^H diag(H_{f,0}, H_{f,1}, \ldots, H_{f,N-1})\mathbf{F}, \tag{3.3.7}$$

$$\begin{aligned} \mathbf{F}\mathbf{H}_T\mathbf{x}_T &= \mathbf{F}\mathbf{F}^H diag(H_{f,0}, H_{f,1}, \ldots, H_{f,N-1})\mathbf{F}\mathbf{x}_T \\ &= diag(H_{f,0}, H_{f,1}, \ldots, H_{f,N-1})\mathbf{x}_f, \end{aligned} \tag{3.3.8}$$

Hence the received signal can be expressed as

$$\mathbf{y}_f = diag(H_{f,0}, H_{f,1}, \ldots, H_{f,N-1})\mathbf{x}_f + \mathbf{n}_f, \tag{3.3.9}$$

where $\mathbf{F}$ is the DFT matrix, subscript f and superscript H denotes the data in frequency domain and Hermitian transpose, respectively. $\mathbf{y}_f$ and $\mathbf{x}_f$ are the received and transmitted data in frequency domain. $\mathbf{n}_f$ is the frequency domain noise. $H_{f,i}$ is the *i-th* coefficient of the DFT channel response. Based on (3.3.9), the transmitted data is scaled by a gain $H_{f,i}$ on each subcarrier of $\mathbf{x}_f$ and the interference from adjacent symbols vanishes.

In general, there are M_t antennas in the transmitter and M_r antennas in the receiver. The interference comes from not only the adjacent symbols but also other antenna signals. The discrete time channel impulse response function is expressed as

$$h_q[n] = \sum_{p=1}^{M_t} \sum_{l=0}^{\nu} h_{q,p}[l]\delta[n-l], \qquad (3.3.10)$$

where $h_{q,p}[l]$ is the complex channel tap coefficient from the *p-th* transmitter antenna to the *q-th* receiver antenna and $\delta[\cdot]$ is delta function. For the OFDM system with cyclic extended guard interval, the channel described in (3.3.10) can be expressed in a matrix form as

$$\mathbf{H}_{\mathrm{T,MIMO}} = \begin{bmatrix} \mathbf{H}_{\mathrm{T},11} & \cdots & \mathbf{H}_{\mathrm{T},1M_t} \\ \vdots & \ddots & \vdots \\ \mathbf{H}_{\mathrm{T},M_r,1} & \cdots & \mathbf{H}_{\mathrm{T},M_r,M_t} \end{bmatrix}, \qquad (3.3.11)$$

where $\mathbf{H}_{\mathrm{T},qp}$ represents the SISO channel from the *p-th* transmitter antenna to the *q-th* receiver antenna.

Based on (3.3.9) and (3.3.10), the received data in frequency domain of the *q-th* antenna can be expressed as

$$\mathbf{y}_{f,q} = \sum_{p=1}^{M_t} \mathbf{H}_{f,qp}\mathbf{x}_{f,p} + \mathbf{n}_{f,q}, \qquad (3.3.12)$$

where $\mathbf{H}_{f,qp}$ is a diagonal matrix and $\mathbf{n}_{f,q}$ is frequency domain noise on *q-th* receiver antenna. In the rest of this section, we concentrate on frequency domain analysis, therefore the subscript *f* will be omitted. When the signal is synchronized without frequency offset, Equation (3.3.12) implies every element in vector $\mathbf{y}_q$ is a linear combination of the same position elements of vectors $\mathbf{x}_1, \mathbf{x}_2, \cdots, \mathbf{x}_{M_t}$ and noise.

Based on this observation, we confine our attention to the *i-th* subcarrier and rewrite the OFDM signal on the *i-th* subcarrier as

$$\underbrace{\begin{bmatrix} y_1 \\ y_2 \\ \vdots \\ y_{M_r} \end{bmatrix}_i}_{\mathbf{y}_i} = \underbrace{\begin{bmatrix} h_{11} & h_{12} & \cdots & h_{1M_t} \\ h_{21} & h_{22} & \cdots & h_{2M_t} \\ \vdots & \vdots & \vdots & \vdots \\ h_{M_r,1} & h_{M_r,2} & \cdots & h_{M_r,M_t} \end{bmatrix}_i}_{\mathbf{H}_i} \underbrace{\begin{bmatrix} x_1 \\ x_2 \\ \vdots \\ x_{M_t} \end{bmatrix}_i}_{\mathbf{x}_i} + \underbrace{\begin{bmatrix} n_1 \\ n_2 \\ \vdots \\ n_{M_r} \end{bmatrix}_i}_{\mathbf{n}_i}, \qquad (3.3.13)$$

where $\mathbf{x}_i$ and $\mathbf{y}_i$ are vectors composed of the *i-th* subcarrier signal of the transmitter and receiver antennas respectively, $\mathbf{n}_i$ is Gaussian noise vector with zero mean and variance σ^2. $\mathbf{H}_i$ is the corresponding channel coefficient matrix that characterizes the coupling between any pair of antennas on *i-th* subcarrier and can be obtained by DFT of (3.3.11). Based on (3.3.13), we can devote our attention to each subcarrier individually and the corresponding per tone equalization scheme can be designed straightforward.

From (3.3.13), we can use linear equalization method to each subcarrier to recover the data. LS and MMSE methods are considered in this section. More noticeworthy is that other equalization method, such as decision feedback equalization (DFE), can be used in the same way.

The optimal LS solution is obtained by using pseudo inverse of $\mathbf{H}_i$

$$\mathbf{W}_{i,LS} = (\mathbf{H}_i^H \mathbf{H}_i)^{-1}\mathbf{H}_i^H, \qquad (3.3.14)$$

where $\mathbf{H}_i^H$ is Hermitian transpose of $\mathbf{H}_i$. $\mathbf{W}_{i,LS}$ is an unbiased estimator and the equalized data is

$$\hat{\mathbf{x}}_{i,LS} = \mathbf{W}_{i,LS}\mathbf{y}_i = (\mathbf{H}_i^H \mathbf{H}_i)^{-1}\mathbf{H}_i^H \mathbf{y}_i. \qquad (3.3.15)$$

Performance of the LS method on slow fading channel can be analyzed by defining the $M_t \times 1$ error vector $\mathbf{e} = \hat{\mathbf{x}}_{i,LS} - \mathbf{x}_i$. We get the

average noise variance as [5]

$$\frac{1}{M_t}\sum_{i=1}^{M_t}|e_i|^2 = \frac{\sigma^2}{M_t}\sum_{i=1}^{M_t}\frac{1}{\lambda_i}, \quad (3.3.16)$$

where λ_i is the eigenvalue of matrix $(\mathbf{H}_i^H \mathbf{H}_i)$. In order to get asymptotic performance, the average signal to noise ratio (SNR) is defined as

$$\mathrm{SNR}_{LS} = \frac{E_s}{\frac{\sigma^2}{M_t}\sum_{i=1}^{M_t}\frac{1}{\lambda_i}}, \quad (3.3.17)$$

where E_s is the average symbol energy. The symbol error probability approximates

$$P_s \approx C \cdot \mathrm{Q}\left(\sqrt{k \cdot \mathrm{SNR}_{LS}}\right), \quad (3.3.18)$$

where $\mathrm{Q}(\cdot)$ is the Q-function defined in [38] and the coefficients C and k depend on the data modulation scheme. For QPSK modulation, C and k are 2 and 0.5, respectively.

The MMSE criterion means to minimize $E\left[\left|x_{i,k} - \mathbf{w}_{i,k}{}^H \mathbf{y}_i\right|^2\right]$, where $\mathbf{w}_{i,k}$ is the equalizer coefficient column vector and E[•] denotes expectation operation. By orthogonality principle, the combining coefficient is designed as

$$\mathbf{W}_{i,MMSE} = [\mathbf{w}_{i,1} \cdots \mathbf{w}_{i,M_t}] = E_s\left(E_s \mathbf{H}_i \mathbf{H}_i^H + \mathbf{R}_n\right)^{-1}\mathbf{H}_i, \quad (3.3.19)$$

for $i = 1,2,...,N$.

And the equalized data are

$$\hat{\mathbf{x}}_{i,MMSE} = \mathbf{W}_{i,MMSE}^H \mathbf{y}_i. \quad (3.3.20)$$

The performance of the MMSE equalizer is analyzed in [38]. It can be shown as

$$\mathrm{SNR}_{MMSE} = \rho\frac{E_s}{\sigma_{\min}^2}, \quad (3.3.21)$$

where

$$\sigma_{\min}^2 = E\left[\left|x_{i,k} - \mathbf{w}_{i,k}^H \mathbf{y}_i\right|^2\right] = E\left[\left|x_{i,k}\right|^2\right] - E\left[\left|\hat{x}_{i,k}\right|^2\right]$$

$$= E_s - \mathbf{w}_{i,k}^H\left(E_s \mathbf{H}\mathbf{H}^H + \mathbf{R}_n\right)\mathbf{w}_{i,k}, \quad (3.3.22)$$

and

$$\rho = \frac{E_s - \sigma_{\min}^2}{E_s} \le 1. \quad (3.3.23)$$

The symbol error rate can be written in terms of the Q-function as

$$P_s \approx C \cdot \mathrm{Q}\left(\sqrt{k \cdot \mathrm{SNR}_{MMSE}}\right). \quad (3.3.24)$$

Again, C and k depend on the data modulation scheme. For QPSK modulation, C and k are 2 and 0.5, respectively.

Based on above discussion, we can depict the receiver in Fig. 3.3.2. In Fig. 3.3.2, the block W_i can be $\mathbf{W}_{i,MMSE}$, $\mathbf{W}_{i,LS}$ or other equalization estimations, such as DFE.

The two-input/ two-output (i.e. $M_t = M_r = 2$) OFDM system is simulated with a bandwidth of 500kHz, divided into 64 subcarriers [40]. The total symbol period is 142 μs, of which 14 μs is cyclic guard interval. Simulation is performed at 500kHz sampling rate, so an OFDM symbol consists 71 (=64+7) samples including 7 samples of guard interval and QPSK modulation is used. The frequency selective channel between any pair of antennas is the six-paths GSM typical urban (TU) model, which has maximum delay spread of 5 μs [39]. The MMSE performance for various power coupling between antennas pairs is simulated and shown in Fig. 3.3.3. Symbol error rate performances for LS, MMSE, and unequalized systems with 3 dB coupling are plotted in Fig.3.3.4.

We summarize this section as follows. We have investigated the OFDM signal in the MIMO frequency selective channel. By means of appending guard interval, a complicated problem of signal coupling among different

antennas and subcarriers can be simplified to a simple matrix form on each subcarrier. Per tone equalization can be designed straightforward. The performance of two-input/two-output OFDM system with LS and MMSE equalization methods are analyzed and simulated. The results are satisfactory.

3.4 Optimal Binary Training Sequence Design for Multiple-Antenna Systems over Dispersive Fading Channels

Efficient channel estimation is important for multiple-antenna systems, especially when the number of antennas increases. To avoid the degradation of estimation accuracy due to interference, an intuitive way is to transmit training sequences for each transmitting antenna in turn [41]. For a system with M antennas, this scheme requires M times bandwidth compared with a single antenna transmitter system. However, orthogonal training sequences can be simultaneously applied for each transmitter antenna to estimate the channel efficiently [25,42]. For a single tap coefficient discrete channel model, it is well known that orthogonal sequences are the optimal training sequences that minimize the estimation errors if the additive noises are identical independent Gaussian random processes. In this case, Hadamard matrice can be applied. However, in the case of multipath channel, channel for each pair of transmitting and receiving antennas should be modeled by several taps. It can be proved that the training sequences should have both good auto-correlation and cross-correlation. Existence of such training sequences sets is still an open problem.

The multiple antenna system under consideration has M transmitting antennas and receiving antennas. The burst data structure for each transmitting antenna is shown in Fig. 3.4.1, where $\underline{x_\alpha(1:L)}$, $\alpha = 1,2,...M$, denotes the training sequence to be transmitted from the αth antenna. L is the length of each training sequence. The training sequences are embedded in each burst. Data bursts from different antennas will have different training sequences, which are designed together so that the coexistence of the training sequences does not affect the channel estimation accuracy. Provided that the burst is short and the channel is quasi-static within a burst, the output of discrete equivalent channel can be expressed as

$$y_\beta(k) = \sum_{\alpha=1}^{M}\sum_{i=0}^{V} h_{\alpha\beta}(i)x_\alpha(k-i) + n_\beta(k), \quad (3.4.1)$$

where V is the order of channel memory, and $h_{\alpha\beta}(i)$ denotes the response of the β^{th} receiving antenna of the receiver to a discrete unit sample applied in the α^{th} transmitting antenna. $n_\beta(k)$ is assumed to be identical independently distributed Gaussian random noise. With good synchronization, small value of V is enough to well approximate the channel. we can prove that the training sequence set is optimal if the training sequence in each antenna is not only orthogonal to its shifts within V taps but also orthogonal to the training sequences in other antennas and their shifts within V taps. In other words, the optimal training sequences should satisfy the

following equation:

$$\sum_{k=1}^{L-V} x_\alpha(k)x_\beta(k+s)=0, \quad \text{where}$$

$$, \ \alpha,\beta=1\sim M; \ s=\begin{cases}0\sim V \text{ when } \alpha\neq\beta \\ 1\sim V \text{ when } \alpha=\beta.\end{cases} \quad (3.4.2)$$

We develop an algorithm to search the existence of the optimal binary sequence satisfy (3.4.2). First, we prove that $x_\alpha(k)=x_\alpha(k+P)$ for $k\leq V$. For convenience, we denote $P=(L-V)$.

In Table 3.4.1, we list the maximal numbers of achievable M given P and V. In the table, N means that no such (P,V,M) code exists. One can observe that the M value for some (P,V) combinations achieve the upper bound given by Property 6, while others do not. For example, when P=16 and V=1, the maximum achievable M is 8, which is just the upper bound given by Property 6. However, when (P,V)=(12,1), the maximal achievable M is only 5, not 6.

In Table 3.4.2, we list at least one example for all existing codes with P≤16. Although we have proved the optimal property of the proposed training seqeunces under the assumption of quasi-coherent channel, we are also interested in their performance in an environment with Doppler frequency shift. We perform numerical simulation to compare three different training sequence sets. The sequences under test are listed in Table 3.4.3. The first one is the optimal sequence set with (P,V,M)=(8,1,4) as proposed. The second sequence set is constructed with a well-known pseudo random binary sequence (PRBS) with different sfhits in different transmitter antennas. Since we want to keep the cross-correlation low between shifts, the maximal number of transmitting antennas is 3 with a PRBS of length 7. The transmitted power is increased to compensate the shorter length for a fair comparison. The third one is an arbitrarily chosen sequence set. The channel tap coefficients are assumed to be independent complex Gaussian random variable with uniformly distributed phase and Rayleigh distributed amplitude. The transmitted power from each transmitting antenna is assumed to be the same. Here, we use the well-known Jakes' model to perform the simulation. The results are shown in Fig. 3.4.2. We see that when the Doppler frequency shift is not severe, the advantage of the proposed sequence set remains unchanged.

3.5 A Robust Timing Synchronization Scheme in Multiple Antenna Systems with Doppler Frequency Shifts

In a multiple antenna system, timing error can cause severer degradation than the single antenna case since intersymbol interference affects all antennas at the same time. Traditionally, symbol timing recovery can be obtained based on the Maximum-likelihood (ML) criterion and implemented in the open-loop or closed-loop form. For example, the well-known early-late gate method and the wave different method (WDM) are closed-loop timing synchronizers [45]. On the other hand, the timing estimator developed in [25] is an open-loop timing estimator for a dual antenna system. However, these estimators are obtained under the assumption of quasi-static channel in the training duration. When the Doppler

frequency shift is severe, the quasi-static assumption may result in significant error such that the performance deteriorates with broadened Doppler bandwidth. Here, we take the time variation of the channel gains into consideration and formulate the multiplicative distortions with linear combinations of their eigenfunctions. Based on this scheme, we derive the ML estimate of the symbol timing. The performance of this scheme is numerically simulated and tested under non-ideal channel state information (CSI) and channel model mismatch. The results show that the proposed scheme outperforms the conventional one.

The communication system under consideration has two transmitting antennas and two receiving antennas. The transmitting antennas send the training signals as

$$x_a(t) = \sum_{k=1}^{L} x_{ak} p(t - kT_s), \quad a = 1,2 \qquad (3.5.1)$$

where L denotes the length of the training sequence, a is the index number of transmitting antenna, T_s is the symbol time duration, x_{ak} is the training sequence, and $p(t)$ is the square-root raised cosine pulse shaping function with roll-off factor ζ. The received signal $z_b(t)$ at receiving antenna b is modeled as

$$z_b(t) = \sum_{a=1}^{2} x_a(t-\varepsilon)\alpha_{ab}(t-\varepsilon) + n_b(t) \quad b = 1,2, \qquad (3.5.2)$$

where $\alpha_{ab}(t)$ is multiplicative distortion, $n_b(t)$ is the additive noise and ε is channel delay. $\alpha_{ab}(t)$ is modeled as zero mean cyclic symmetric complex Gaussian random process having identical autocorrelation function [25] as

$$R_a(t,u) = E[\alpha_{ab}(t)\alpha_{ab}^{*}(u)] = \sigma_a^2 J_0(2\pi f_d(t-u)), \qquad (3.5.3)$$

where $E[\cdot]$ denotes the expectation over the ensembles, * means complex conjugate, $J_0(\cdot)$ represents the zero order Bessel function of the first kind, f_d is the maximum Doppler frequency, and $n_b(t)$ is cyclic symmetric white Gaussian random processes with autocorrelation function $R_n(t,u) = N_0\delta(t-u)$. In addition, all of these random processes are assumed to be independent. As in [46], it is possible to find the eigenfunctions, $f_k(t)$, which satisfy

$$\int_{T_i}^{T_f} R_a(t,u) f_k(u) du = \lambda_k f_k(t), \qquad (3.5.4)$$

where λ_k are the corresponding nonnegative real eigenvalues. T_i and T_f are the initial time and final time of the observation duration, respectively. $f_k(t)$ and λ_k are obtained numerically by approximating (3.5.4) with a discrete one with sufficient resolution. Then, we transform it into the matrix form and find the eigenvectors and eigenvalues of the autocorrelation matrix [47,48]. Assuming $\lambda_k \geq \lambda_{k+1}$, $\alpha_{ab}(t)$ can be expressed as

$$\alpha_{ab}(t) = \lim_{M \to \infty} \alpha_{abM}(t), \qquad (3.5.5)$$

where
$$\alpha_{abM}(t) = \sum_{k=1}^{M} c_{abk} f_k(t), \qquad (3.5.6)$$

and c_{abk} is complex Gaussian random variable with variance λ_k. Now, our objective is to estimate the channel delay ε given the received signal, $z_b(t), b = 1,2$. By an extension to the derivation in [38] and that $n_b(t)$ and c_{abk} are independent, we can get the joint probability density function of c_{abk} and ε, conditioned on $z_b(t)$ and $x_a(t)$. By taking logarithm of the probability density function and neglecting irrelevant constants and scaling, we obtain the likelihood function Γ as

$$\Gamma = \lim_{M\to\infty} -\{\sum_{b=1}^{2}(\frac{1}{N_0}\int_{T_i}^{T_f}|n_b(t)|^2dt + \sum_{k=1}^{M}\sum_{a=1}^{2}|c_{abk}|^2/\lambda_k)\} \quad (3.5.7)$$

Now, we can apply (3.5.2) (3.5.5) (3.5.6) and rewrite the last term of (3.5.7) in matrix form to obtain

$$\Gamma = \lim_{M\to\infty}\Gamma_M, \quad (3.5.8)$$

$$\Gamma_M = -\{\sum_{b=1}^{2}(\frac{1}{N_0}\int_{T_i}^{T_f}\left|z_b(t+\varepsilon) - \sum_{a=1}^{2}x_a(t)\alpha_{abM}(t)\right|^2 dt + \sum_{a=1}^{2}C_{abM}^H\Lambda_M^{-1}C_{abM})\}, \quad (3.5.9)$$

where C_{abM} and Λ_M are a column vector and a diagonal matrix given by $C_{abM} = [c_{ab1}\ c_{ab2}\ \cdots\ c_{abM}]^T$ and $\Lambda_M = diag(\lambda_1, \lambda_2, .., \lambda_M)$. The superscripts T and H denote the transpose and Hermitian transpose, respectively. Here, we have used the fact that a shift in $n_b(t)$ does not change its statistical property. To maximize Γ_M, we obtain the ML channel estimate as

$$C_{bM} = (R + N_0\Lambda_{M2}^{-1})^{-1}V_{bM}(\varepsilon), \quad (3.5.10)$$

where $C_{bM} = [C_{1bM}^T\ C_{2bM}^T]^T$ and $\Lambda_{M2} = diag[\Lambda_M\ \Lambda_M]$. R is a $2M\times 2M$ matrix with elements r_{mn} given by

$$r_{mn} = \int_{T_i}^{T_f} x_{a_1}(t)f_{k_1}(t)x_a^*(t)f_k^*(t)dt, \quad (3.5.11)$$

where $m = (a-1)M + k$, $n = (a_1 - 1)M + k_1$, $a, a_1 = 1\sim 2$, $k, k_1 = 1\sim M$. $V_{bM}(\varepsilon)$ is defined as

$$V_{bM}(\varepsilon) = [v_{b11}\ v_{b12}\ ..v_{b1M}\ v_{b21}\ v_{b22}\ ..v_{b2M}]^T, \quad (3.5.12)$$

where $v_{bak} = \int_{T_i}^{T_f} z_b(t+\varepsilon)x_a^*(t)f_k^*(t)dt$. (3.5.13)

Based on (3.5.5) through (3.5.13), we find the ML estimate of ε as

$$\varepsilon_{ML} = \arg\max_{\varepsilon}\{\lim_{M\to\infty}\sum_{b=1}^{2}[V_{bM}^H(\varepsilon)(R + N_0\Lambda_{M2}^{-1})^{-1}V_{bM}(\varepsilon) - \int_{T_i}^{T_f}|z_b(t+\varepsilon)|^2dt]\}. \quad (3.5.14)$$

Note that the last term in (3.5.14) is independent of ε for proper choices of T_i and T_f. As a result, (3.5.14) is simplified as

$$\varepsilon_{ML} = \arg\max_{\varepsilon}[\lim_{M\to\infty}\sum_{b=1}^{2}V_{bM}^H(\varepsilon)(R + N_0\Lambda_{M2}^{-1})^{-1}V_{bM}(\varepsilon)] \quad (3.5.15)$$

Depending on the bandwidth of the random process, it is sufficient to well approximate $\alpha_{ab}(t)$ with a small M [46]. Therefore, with an appropriate value of M, the limit operation in (3.5.15) can be removed with only negligible degradation in performance. We find that for normalized maximum Doppler frequency, $f_n = f_d T_s$, less than 0.05, the first two eigenvalues consist of more than 85% of the total energy. In the following simulations, we show that with $M = 2$, the estimation error is greatly reduced compared with the conventional ML based on quasi-static assumption for normalized maximal Doppler frequency f_n as large as 0.06.

The conventional scheme uses simple correlation to acquire the estimate of ε [25]. This is equivalent to have $M = 1$ and approximate $f_1(t)$ as a constant function in (3.5.6) without the limit operation in (3.5.5). In Fig. 3.5.1, we compare the proposed scheme with $M = 2$ to the conventional correlation approach. The parameters of the simulation are given as follows. The roll-off factor is 0.3, and the pulse shaping function $p(t)$ is truncated to $\pm 3T_s$ around $t = 0$. The continuous waveform is represented by 32 samples per symbol. The acquisition interval is assumed to be $\pm 1.5T_s$ around the correct timing delay. The orthogonal

training sequence pair are x_{1k} = [+−−−−+−−++ +−] and x_{2k} = [++−++−−−−+−++]. We can see that the conventional approach deteriorates seriously as the maximum Doppler frequency shift increases while the proposed method retains reasonable performance. We can see that for normalized frequency as large as 0.05, the proposed method with Es/No= 4 dB has the same performance as the conventional method with Es/No=10 dB. The improvement is more significant at high SNR.

As suggested in (3.5.15), the timing synchronization requires the knowledge of signal to noise ratio and the maximum Doppler frequency shift. Thus, we investigate sensitivity of the proposed method to the non-ideal CSI. In Fig. 3.5.1, we plot the performance of the proposed method with non-ideal information of SNR. The systems are designed with Es/No 8dB or 20 dB larger than or lower than the actual Es/No. Fig. 3.5.2 depicted the performance of the estimators with a fixed design value of f_n in various Doppler frequency spread environments. In addition, we also investigate the effect of model mismatch. We feed white noise into ideal lowpass filters to obtain the multiplicative distortion $\alpha_{ab}(t)$ while the system is designed under assumption of Jakes Doppler spectrum with $f_n = 0.03$. The results are compared to the conventional correlation approach and illustrated in Fig. 3.5.3. It shows that the proposed method is also insensitive to model mismatch. The reason for the insensitivity of model mismatch is explained as follows. The first eigenfunction is very close to a constant and the second eigenfunction is similar to a straight line. The mismatched model just changes the corresponding eigenvalues so that the importance of each component is slightly mis-weighted.

Since this scheme is insensitive to model mismatch and CSI, we can choose the average value of the SNR and f_n for the target operating environment. Thus, we can find $f_k(t)$ and compute $(R + N_0\Lambda_{M2}^{-1})^{-1}$ beforehand and store them in ROM. Special care can be taken to make non-diagonal elements of $(R + N_0\Lambda_{M2}^{-1})^{-1}$ negligibly small to reduce the computation. $V_{bM}(\varepsilon)$ must be calculated via (3.5.12) and (3.5.13) in real time, which dominate the computational complexity of this scheme. Compared to the conventional correlation method with the same oversampling ratio, it takes approximately two-fold multiplications and additions for $M = 2$.

3.6 Performance Analysis of 16 QAM OFDM Transmission with Polarization Diversity Over Dispersive Fading Channel

For the OFDM scheme, the longer symbol duration can reduce the inter-symbol interference (ISI). Meanwhile, the spectrum of an individual sub-channel normally occupies only a small portion of the available bandwidth in which the quadrature amplitude modulation (QAM) can be used to increase the bandwidth efficiency. On the other hand, the dual polarization frequency reuse system can theoretically double the system capacity [12].

However, in practice, impairments such as multi-path fading, antenna misalignment, and cross polarization interference, may cause serious performance degradation [49][50]. For mobile communications, the channel has time-varying characteristic. Channel estimation is important. It is known that the pilot symbol assisted modulation (PSAM) in which the predetermined pilot symbols are periodically inserted into the transmitting stream is better than the pilot tone assisted modulation.

Here, we will propose and analyze the 16QAM OFDM transmission with polarization diversity over the dispersive fading channel. This transmission system utilizes PSAM to improve the error performance. We derive the optimum interpolation coefficients by using the time domain autocorrelation function of the fading channel. The result shows that our system performs better than others.

Fig. 3.6.1 shows the transmitter structure of the proposed system. Assuming N as the number of sub-channels, we convert the data stream into N branches by a serial to parallel converter (SPC). In each branch the data stream is split again into two parallel sub-branches by the next stage SPC. Then the sub-branch stream is fed into the signal mapper, which maps the input binary data into 16QAM symbols. The predetermined PSAM symbol for the particular sub-branch is inserted into the symbol sequence at the beginning of every (M-1) symbols to form a frame prior to pulse shaping. Thus, for each sub-branch, the frame size is M.

After pulse shaping, the signals of the two sub-branches of the ith sub-channel are up-converted to the corresponding radio frequencies with different polarizations, f_{iH} and f_{iV}, H and V denote the horizontal and vertical polarizations, respectively. Without loss of generality, linear polarization is assumed. To maintain orthogonality between sub-carriers, $f_{iH,}$, f_{iV}, $i = 1,..., N$ the sub-carrier spacing is chosen carefully to be the symbol rate [1].

Fig. 3.6.2 shows the schematic of the receiver. At the output of the match filter of each sub-branch, the pilot symbols are extracted by decimation operation in the channel estimator, and then are interpolated to form an estimate of the channel state. The demodulator uses the channel state information to compensate the fading effect on the data symbol.

The channel model including cross polarization and fading interferences is shown in Fig. 3.6.3, where γ_V and γ_H represent the power coupling coefficients, f_D is the Doppler frequency, $n_H(t)$ and $n_V(t)$ are additive white Gaussian noises with zero mean and power spectral density $N_0/2$.

At the transmitter, the horizontal and vertical polarized signals are given by

$$S_H(t) = \sum_{i=1}^{N} \sum_{k=-\infty}^{\infty} b_{iH}(k) p(t - kT) e^{j2\pi f_{iH} t} \quad (3.6.1)$$

and

$$S_V(t) = \sum_{i=1}^{N} \sum_{k=-\infty}^{\infty} b_{iV}(k) p(t - kT) e^{j2\pi f_{iV} t}, \quad (3.6.2)$$

where $b_{iH}(k)$ and $b_{iV}(k)$ are the symbols taken from the constellation of the 16QAM scheme in the *ith* sub-carrier of the *kth* symbol, T is the OFDM symbol duration, $p(t)$ is the impulse response of the pulse shaping filter and is assumed to have unit energy. The received signal at the horizontal polarized antenna is

expressed as

$$m_H(t) = [\sqrt{1-\gamma_H}\, S_H(t) z_H(t) + \sqrt{\gamma_V}\, S_V(t) z_V(t)] e^{j2\pi f_D t} + n_H(t), \qquad (3.6.3)$$

where $z_H(t)$ and $z_V(t)$ are the complex fading distortion gains with variances σ_H^2 and σ_V^2. For simplicity, we assume that the two polarizations are symmetric, i.e. $\gamma_H = \gamma_V = \gamma$. When γ gets larger, the power of the desired symbol becomes smaller. The system performance for various values of γ is shown in Fig. 3.6.4. In conventional dual polarization transmission systems, the system performance degrades seriously by the interference. However, due to one more orthogonal dimension in the frequency domain, the coupling has little affection on the SER of the proposed system.

The spacing between the pilot symbols should be chosen small enough to perform good estimate of the fading channel state but large enough without increasing the overhead. Fig. 3.6.5 shows the effect due to the pilot spacing which is equivalent to the frame length at the interpolation size 63, $\gamma = 0.2$ and $E_b/N_0 = 30dB$. As shown, even in severe Doppler spread, the frame length doesn't have serious impact on the system performance when it is smaller than eight. Therefore, in this report, the selected frame length is six, which implies the predetermined symbol, inserted at every five data symbols. Note that the sharp rise in SER appears when the pilot spacing is so long that the sampling rate is lower than the Nyquist rate, i.e., when $\frac{1}{MT} < 2f_D$.

The system performance versus the interpolation size is shown in Fig. 3.6.6. The system performs satisfactory as interpolation size is larger than about thirteen, when γ and fdT are 0.2 and 0.01. This implies that the estimator can get enough information about the fading channel from the pilot symbols to perform reasonable estimation. Thus, in our system, the interpolation size is chosen as thirteen.

The performance for various value of normalized Doppler spread is depicted in Fig. 3.6.7. In which, even in serious Doppler spread, there is no significant degradation. The performance comparison of the proposed system and the systems with MMSE estimate and linear interpolation in transform domain [50], is shown in Fig. 3.6.8. These examples show that the system performance is still satisfactory even in severe interference environment.

3.7 MC-MLSE of Space-Time Coded Signals over Dispersive Channels

This section investigates the equalization for space-time coded signals with transmission diversity over frequency selective channels. We derive a multi-channel maximum likelihood sequence estimator (MC-MLSE) jointly with space-time decoding process for both hard and soft decisions. We first consider the discrete time signal model and system details. Moreover, a discussion then arises about the MC-MLSE algorithm and its performance evaluation. Simulation results show that the proposed

system operates at a satisfactory level of performance compared with maximum a posterior (MAP) equalization.

The sketch of multiple input / multiple output (MIMO) system under consideration is shown in Fig. 3.7.1, which has N_t transmitting antennas in the transmitter and N_r receiving antennas in the receiver over a frequency selective Rayleigh fading environment. The impulse response of the discrete time equivalent channel for overall system between the i-th transmitting antenna to the j-th receiving antenna is modeled by a time-varying FIR response as:

$$\alpha_{ij}(k) = \sum_{d=0}^{D} a_{ij}(k,d)\delta(k-d) \qquad (3.7.1)$$

where the tap gains $a_{ij}(k,d)$ are modeled as i.i.d. complex Gaussian random variables with zero mean and variance $\sigma_a^2(d)$, D is the order of channel memory and k denotes the time instance kT. The impulse response includes the effects of the transmitter pulse shaping filter, the receiver front-end filter, the physical multipath propagation channel and symbol-spaced sampler between the i-th transmitting antenna to the j-th receiving antenna. Moreover the channel is assumed to be passive and normalized, such that

$$\sum_{d=0}^{D} \sigma_a^2(d) = 1. \qquad (3.7.2)$$

At a given time instance k, let $s(k)$ be the input to the encoder and let the corresponding output of space-time encoder be $\{c_1(k), c_2(k), \cdots, c_{N_t}(k)\}$, where the code symbol $c_i(k)$ is transmitted from Antenna i, $i = 1,2,\cdots N_t$. Then we can write the received signal at receiving Antenna j under the assumption of slowly fading channels as follows

$$r_j(k) = \sum_{i=1}^{Nt}\sum_{d=0}^{D} a_{ij}(d)c_i(k-d) + n_j(k)$$

$$, \quad 1 \le j \le Nr. \qquad (3.7.3)$$

The term $n_j(k)$ is the sequence of i.i.d. complex Gaussian noise samples with zero mean and variance σ_n^2.

More compactly, we express the output vector of N_r receiving antennas as

$$\underline{\mathbf{r}}(k) = [r_1(k), r_2(k), \ldots\ldots\ldots, r_{Nr}(k)]^{\mathrm{T}}$$

$$= \sum_{i=1}^{Nt} \underline{\underline{\mathbf{H}}}_i \underline{\mathbf{c}}_i(k) + \underline{\mathbf{n}}(k) \qquad (3.7.4)$$

$$\text{where } \underline{\underline{\mathbf{H}}}_i = [\underline{\mathbf{a}}_{i1}, \underline{\mathbf{a}}_{i2}, \ldots\ldots\ldots, \underline{\mathbf{a}}_{iN_r}]^{\mathrm{T}} \qquad (3.7.5)$$

$$\underline{\mathbf{n}}(k) = [n_1(k), n_2(k), \ldots\ldots\ldots, n_{Nr}(k)] \qquad (3.7.6)$$

$$\underline{\mathbf{a}}_{ij} = [a_{ij}(0), a_{ij}(1), \ldots\ldots\ldots, a_{ij}(D)] \qquad (3.7.7)$$

$$\underline{\mathbf{c}}_i(k) = [c_i(k), c_i(k-1), \ldots\ldots\ldots, c_i(k-d)]^{\mathrm{T}}. \qquad (3.7.8)$$

The noise vector $\underline{\mathbf{n}}(k)$ has zero mean and covariance matrix $\underline{\underline{\mathbf{R}}}_n = \sigma_n^2 \cdot \underline{\underline{\mathbf{I}}}_{N_r \times N_r}$.

As a result, Eq. (3.7.4) will be served as the received signal expression for developing equalization techniques.

We consider that the channel is slowly time-variant, i.e. the multipath parameters are invariant within a data burst. We define the distance function as

$$D^2(k) = \left\| \underline{\mathbf{r}}(k) - \sum_{i=1}^{Nt} \underline{\underline{\mathbf{H}}}_i \underline{\mathbf{c}}_i(k) \right\|^2. \qquad (3.7.9)$$

Then the likelihood of $\{\underline{\mathbf{r}}(0), \underline{\mathbf{r}}(1), \cdots, \underline{\mathbf{r}}(K-1)\}$

given $\{\underline{\mathbf{c}}_i(0),\underline{\mathbf{c}}_i(1),\cdots,\underline{\mathbf{c}}_i(K-1)\}_{i=1}^{N_t}$ is proportional to $\exp\{-1/2\sigma_n^2 \cdot \sum_{k=0}^{K-1} D^2(k)\}$ [38] where K is the total number of information symbols. Hence, we may find a sequence of vectors $\{\underline{\mathbf{c}}(0),\underline{\mathbf{c}}(1),\cdots,\underline{\mathbf{c}}(K-1)\}$ where $\underline{\mathbf{c}}(k)=[c_1(k),c_2(k),\cdots,c_{N_t}(k)]^T$ which minimizes

$$\sum_{k=0}^{K-1} D^2(k) = \sum_{k=0}^{K-1} \left\| \underline{\mathbf{r}}(k) - \sum_{i=1}^{N_t} \underline{\underline{\mathbf{H}}}_i \underline{\mathbf{c}}_i(k) \right\|^2 . \quad (3.7.10)$$

Because each sequence of the transmitted code vectors $\{\underline{\mathbf{c}}(0),\underline{\mathbf{c}}(1),\cdots,\underline{\mathbf{c}}(K-1)\}$ represents a path through the trellis, the MC-MLSE searches the most likely path based on the observation vectors $\{\underline{\mathbf{r}}(0),\underline{\mathbf{r}}(1),\cdots,\underline{\mathbf{r}}(K-1)\}$. In other words, the main task of the MC-MLSE is to compute the accumulated branch metrics associated with the state transitions in the channel trellis among all possible paths. The search can be done by Viterbi algorithm resulting from the concept of dynamic programming [56].

We will present the fact that the performance of MC-MLSE can approach the matched filter bound (MFB) with the aid of the whiten matched filter (WMF). The MC-MLSE can transform the dispersive channel to a decoupled one with a channel gain (nonrandom) standing for the total energy of dispersive channel taps and additive noise. The performance of the MC-MLSE is superior to the traditional linear equalizer techniques for the reason that it can gather all energy of channel taps as path diversity gain to reduce the required signal level.

For the j-th receiving antenna, the equivalent model of the MC-MLSE can be simplified as shown in Fig. 3.7.2.

To achieve the MFB with transmit diversity as the limit of the system performance, the relation between the complex channel gain α_{ij} and the dispersive sub-channel $\underline{\mathbf{h}}_{ij}$ is given by

$$|\alpha_{ij}|^2 = \|\underline{\mathbf{h}}_{ij}\|^2 . \quad (3.7.11)$$

We define the diversity gain as

$$\mu_j^2 = \sum_{i=1}^{N_t} |\alpha_{ij}|^2 = \sum_{i=1}^{N_t} \|\underline{\mathbf{h}}_{ij}\|^2 . \quad (3.7.12)$$

Accordingly, it is straightforward to show that the SNR at the output of the j-th receiving antenna is

$$\gamma_j = \frac{\mu_j^2 \cdot E_s}{\sigma^2} . \quad (3.7.13)$$

where E_s is the symbol energy, and σ^2 is noise power

We further assume that α_{ij} is a set of i.i.d. complex Gaussian random variables with zero mean and variance σ_α^2. Hence, the output SNR is a N_t-th order Erlang random variable with mean $\frac{N_t}{\beta}$ and variance $\frac{N_t}{\beta^2}$ where $\beta = \frac{\sigma^2}{E_s \cdot \sigma_\alpha^2}$ [38].

For the QPSK signaling, the associated bit error rate averaged over the random distribution of received SNR takes the form

$$P_b(N_t) = \frac{1}{2} \cdot \{1 - (\frac{1}{\sqrt{2\beta+1}}) \cdot [\sum_{k=0}^{N_t-1} \binom{2k}{k} (\frac{\beta}{4\beta+2})^k]\}. \quad (3.7.14)$$

Eq. (3.7.14) provides a theoretical MFB on the MC-MLSE with transmit diversity N_t. Fig. 3.7.3 depicts the bit error performance versus SNR for different N_t.

The proposed system has the disadvantage that it suffers from the loss of the information for space-time decoding process due to the hard decisions at the output of the equalizer. Therefore the performance degrades without taking full advantage of the space-time coding. The soft decoding scheme can be used to improve the system performance. We employ the trellis refinement because both Viterbi equalizer and space-time encoder possess the trellis structure. It is natural to take the combination of space-time trellis code with channel trellis into consideration. We note that there are only Z branches (Z is the constellation size) from and to each state for soft decisions instead of Z^{N_t} transitions for hard decisions and the corresponding input label of the equalizer trellis for soft processing is the information symbol $s(k)$ rather than the codeword vector $\underline{\mathbf{c}}(k)$ for hard decoding. The reduction of state transitions is due to the fact that some possible branches in the equalizer trellis for hard decoding are denied by the space-time coding trellis and it leads to the reduction of computation complexity.

The multi-channel Viterbi equalizer for both soft and hard decoding with QPSK 4-state space-time code is applied the two-input / two-output system. We assume that each subchannel has 2 taps with equal energy and its parameters do not change within a frame with 400 QPSK symbols long. In addition, perfect knowledge of channel state information is known at the receiver.

Fig. 3.7.4 shows the performance of the MC-MLSE equalizer of space-time coded signals for both soft and hard decoding. There is a 14dB improvement of E_s / N_0 for soft decoding process at SER 10^{-3} over hard decisions. Compared to the turbo MAP equalizer at the same performance level, the required E_s / N_0 is roughly about 15 dB with random interleaving and one iteration (feedback) [57]. Hence a 5dB advantage is gained for soft decoding.

Fig. 3.7.5 shows the performance of space-time coded transmission with MC-MLSE for hard decisions, which is worse than the MFB due to the information loss of hard-cut decisions. On the contrary, the performance for soft decoding is 5 dB better than MFB at 10^{-3} BER with the aid of well-designed space-time codes. Moreover, we present the frame error rate of space-time coded transmission with the MC-MLSE for both soft and hard decoding as shown in Fig. 3.7.6.

4. Self Evaluation

本計畫研究內容確實地完成了原計畫的進度，並由原來偏極化載波應用引伸出至多維天線傳輸，許多研究已發表於著名國際期刊或國際會議，成果頗豐。

5. Conclusion

According to the research results, using dual polarized waves can largely increase the spectrum efficiency with the cost of higher hardware cost and complicated signal processing. The availability of mobile communication can be significantly improved using antenna diversity with space-time coding. These schemes can also be applied to wireless local area network to increase the transmission data rate. The recent news says that Agere has implement a wireless LAN MIMO-OFDM system which increase the transmission data rate to 162 Mbps using the IEEE 802.11a standard spectrum which use 20 MHz for each channel. This is a proof of technical feasibility of multiple antenna system. As the demand for wireless communication increases and the available spectrum remains limited resource, it is quite possible that the future generation of communication may utilize the multiple antenna technology.

6. Reference

[1] Jingshown Wu and Meng-Che Wu, "Dual-Polarization Frequency Reuse with Frequency Band Shifting Allocation ", IEEE Transactions on Vehicular Technology, Vol.49,No.6,PP.2244-2256 , Nov 2000

[2] Jingshown Wu and Shan-An Yang, "Dual Polarization Waves Reuse Scheme in Cross Polarization Channel", IEEE GLOBECOM'99, pp.2714-2718, Rio, Brazil, Dec. 5-9, 1999

[3] Shan-An Yang and Jingshown Wu, "A New Dual Polarization Wave Reuse Communication System for Cross Polarization and Antenna Misalignment Channel" has been submitted for IEEE Transaction on Communication, under revision.

[4] T.H. Chou and J. Wu, "A New Per Tone Equalization Structure for MIMO OFDM System", IASTED International Conference AIC 2001, Rhodes, Greece, July 3-6, 2001.

[5] Shan-An Yang and Jingshown Wu, "Optimal Binary Training Sequence Design for Multiple-Antenna Systems over Dispersive Fading Channels" has been accepted for publication in IEEE Transaction on Vehicular Technology.

[6] Shan-An Yang and Jingshown Wu, "A Robust Timing Synchronization Scheme in Multiple Antenna Systems with Doppler Frequency Shifts" has been accepted for publication in IEEE Communications Letters.

[7] Jingshown Wu and Nan-Jung Wei, "Performance Analysis of 16 QAM OFDM Transmission with Polarization Diversity Over Dispersive Fading", submitted to the IEEE Transactions on

Vehicular Technology, under revision.

[8] Jingshown Wu and Weinan Sun, "MC-MLSE of Space-Time Coded Signals over Dispersive Channel", International Symposium on Communications, Nov 2001

[9] W. Y. Zou, and Yiyan Wu, "COFDM: An Overview, " IEEE Transaction on Broadcasting, vol. 41, no. 1, pp. 1-8, March 1995.

[10] H.H. H'mimy, "Channel Estimation Based on Coded Pilot for OFDM," IEEE Vehicular Technology Conference, vol. 3, pp.1375 –1379, 1997.

[11] D.T. Harvatin, and R.E. Ziemer, "Orthogonal Frequency Division Multiplexing Performance in Delay and Doppler Spread Channels," IEEE Vehicular Technology Conference, vol. 3, pp.1644 -1647, 1997.

[12] C.E. Hendrix, G. Kulon, C.S. Anderson, and M.A. Heinze, "Multigigabit Transmission Through Rain in a Dual Polarization Frequency Reuse System: An Experimental Study," IEEE Transactions on Communications vol. 41, no. 12, pp.1830 -1837, Dec. 1993.

[13] L. Ordano, and F. Tallone, "Dual Polarised Propagation Channel: Theoretical Model and Experimental Results," Antennas and Propagation, Tenth International Conference on, vol. 2, pp.363-366, April 1997.

[14] T. S. Chu, "Restoring the Orthogonality of Two Polarizations in Radio Communication Systems I," Bell Syst. Tech. J., vol. 50, no. 9, pp. 3063-3069, Nov. 1971.

[15] T. S. Chu, "Restoring the Orthogonality of Two Polarizations in Radio Communication Systems II," Bell Syst. Tech. J., vol. 52, no. 3, pp. 3063-3069, March 1973.

[16] B. Lankl, J.A. Nossek, and G. Sebald, "Cross-Polarization Interference in the Presence of Delay Effects," Communications ICC '88. Digital Technology - Spanning the Universe. Conference Record vol.3. IEEE International Conference on , pp.1355-1361, 1988.

[17] M. Kavehrad, and J.Salz, "Cross-Polarization Cancellation and Equalization in Digital Transmission Over Dually Polarized Multipath Fading Channels," Bell Syst. Tech. J., vol. 64, no. 10, pp.2211-2245, Dec. 1985.

[18] Parsons, The Mobile Radio Propagation Channel, New York: Wiley.

[19] J.G. Proakis, Digital Communications, 2nd ed., New York: McGraw-Hill, 1989, May 1993.

[20] Hongya Ge, Y. Bar-Ness, and M. Visser, "Combined Adaptive Interference Cancellation and Bootstrap Separation of Dual Polarized Signals," Signals, Systems and Computers, 1996. Conference Record of the Thirtieth Asilomar Conference on vol. 1, pp.694-698, 1996.

[21] G. Santella, "Bit Error Rate Performances of M-QAM Orthogonal Multicarrier Modulation in Presence of Time-Selective Multipath Fading ," IEEE ICC '95, Seattle, 'Gateway to Globalization', International

Conference on vol. 3, pp.1683 –1688, vol.3, 1995.

[22] S. Benedetto, "Theory of Polarization Shift Keying Modulation",IEEE Transaction on Communication, Vol. 40, No. 4, pp 708-721 , April, 1992.

[23] Rocha, Armando "Two XPD frequency scaling models using quasi-physical parameters to characterize earth satellite propagation channel", Proceedings of IEEE AP-S International Symposium, Canada, pp 2548-2551, July, 1997

[24] H. V. Bazak, "Simple depolarization compensator for a very wideband communications links - an experimental evaluation.," IEEE Transactions on Communications Vol. 42, No. 5, pp. 2073-2077,May, 1994

[25] Ayman F. Naguib, Vahid Tarokh, Nambirajan Seshadri, and A. Robert Calderbank, "A Space-Time Coding Modem for High-Data-Rate Wireless Communications", IEEE Journal on Selected Areas in Communications, Vol. 16, No. 8, pp. 1459-1477, Oct. 1998.

[26] Vahid Tarokh, Nambi Seshadri, and A. R. Calderbank, "Space-Time Codes for High Data Rate Wireless Communication: Performance Criterion and Code Construction", IEEE Transactions on Information Theory, Vol. 44, No. 2, pp. 744-765, Mar. 1998.

[27] Zhihong Zhao, Shawn Stapleeton and James K Cavers, "Analysis of Polarization Diversity Scheme with Channel Codes", Proceedings of IEEE Vehicular Technology Conference, pp1377-1381, Amsterdam, The Netherlands, Sept., 1999.

[28] Jean Philippe Kermoal, Laurent Schumacher, Frank Frederiksen, and Preben E. Mogensen, "Polarization Diversity in MIMO Radio Channels, Experimental Validation of a Stochastic Model and Performance Assessment", Proceedings of IEEE Vehicular Technology Conference, pp.22-26, Atlantic City, USA, Oct. 2001.

[29] Zhuo Chen, Branka Vucetice, Jinhong Yuan and Ka Leong Lo, "Space-time Trellis Codes with Two, Three and Four Transmit Antennas in Quasi-Static Flat Fading Channels", Proceedings of ICC. 2002, Vol. 3, pp.1589-1595.

[30] David K. Cheng, Field and Wave Electromagnetics, 2nd, 1989, Addison Wesley, U.S.A.

[31] G. J. Foschini and M. J. Gans, "On limits of wireless communications in a fading environment when using multiple antennas", Wireless Personal Communications, Vol 6, pp. 311-335, 1998.

[32] A. Duel-Hallen, "Equalizers for multiple input/multiple output channels and PAM systems with cyclostationary input sequences", IEEE J. Select. Areas Commun., vol. 10, pp. 630-639, April 1992.

[33] L. Vandendorpe, O. van de Wiel, "MIMO DFE equalization for multitone DS/SS systems over multipath channels", IEEE J. Select. Areas Commun., vol.14, pp. 502-511, April 1996.

[34] J.K. Tugnait, B. Huang, "On a whitening

approach to partial channel estimation and blind equalization of FIR/IIR multiple-input multiple-output channels", IEEE Trans. Signal Processing, vol. 48, pp.832-845, March 2000.

[35] A. Chevreuil, L. Vandendorpe, "MIMO MMSE-DFE: a general framework", Statistical Signal and Array Processing, Ninth IEEE SP Workshop, pp. 368-371, 1998.

[36] A. Maleki-Tehrani, B. Hassibi, J.M. Cioffi, "Adaptive equalization of multiple-input multiple-output (MIMO) channels", Communications, 2000. ICC 2000, vol. 3, pp. 1670 –1674, 2000.

[27] Gilbert String, Linear algebra and its applications, 3rd ed., San Diego: Harcourt, Brace, Jovanovich, Publishers, 1988.

[38] J. G. Proakis, Digital Communications, 3rd ed., New York: McGraw-Hill, 1995.

[39] K. Pahlavan and A. H. Levesque, Wireless Information Networks. New York: Wiley, 1995.

[40] J. J. van de Beek, O. Edfors, M. Sandell, S. K. Wilson, and P. O. Borjesson, On channel estimation in OFDM systems, in Proc. IEEE Vehicular Technology Conf., vol. 2, July 1995, pp. 815–819.

[41] Roberto Cusani, Enzo Baccarelli, Guido Di Blasio, and Stefano Galli, "A Simple Polarization-Recovery Algorithm for Dual-Polarized Cellular Mobile-Radio Systems in Time-Variant Faded Environments", IEEE Transactions on Vehicular Technology, vol. 49, no. 1, pp. 220~228, January 2000.

[42] M. Kavehrad, "Performance of Cross-Polarized M-ary QAM Signals Over Nondispersive Fading Channels", AT&T Bell Laboratories Technical Journal, vol. 63, no. 3, pp. 499-521, March 1984.

[43] Jacques Wolfmann, "Almost Perfect Autocorrelation Sequences", IEEE Transactions on Information Theory, vol. 28, no. 4, pp.1412~1418, July 1992.

[44] Alexander Pott and Steven P. Bradley, "Existence and Nonexistence of Almost-Perfect Autocorrelation Sequences", IEEE Transactions on Information Theory, vol. 41, no. 1, pp. 301~304, January, 1995.

[45] G. O. Y S. F. Hau and C. Y. Chan, "The Use of WDM for Timing Synchronization in Rayleigh Fading Channel", Proc. ICSP, pp1640-1645, Seattle, May, 1998.

[46] Landau H.J., Pollak H.O., "Prolate spheroidal wave functions, Fourier analysis and uncertainty. II", Bell System Tech. J. vol. 40, pp. 65-84, 1961.

[47] Grünbaum F. Alberto, "Eigenvectors of a Toeplitz matrix: discrete version of the prolate spheroidal wave functions.", SIAM J. Algebraic Discrete Methods vol. 2, no. 2, pp. 136-141, 1981.

[48] Grünbaum F. Alberto,"Toeplitz matrices commuting with tridiagonal matrices", Linear Algebra Application, vol. 40, pp.25-36, 1981

[49] C. E. Hendrix, J. E. Mcnally, and R. A. Monzingo, "Depolarization and attenuation effects of radomes at 20Ghz, " IEEE Trans. Antennas Propagat. , vol. 37, pp. 320-328, March. 1989.

[50] O. Edfors, M. Sandell, J.-J. vande Beek, S.

K. Wilson, and P. O. Borjesson, "OFDM channel estimation by singular value decomposition, " IEEE Trans. Commun. , vol. 46, pp. 931-939, July. 1998.

[51] J. K. Cavers, " An analysis of pilot symbol assisted modulation for Rayleigh fading channels, " IEEE Trans. Vehic. Tech. , vol. 40, pp. 686-693, Nov. 1991.

[52] P. Balaban and J. Salz, "Optimum diversity combining and equalization in data transmission with application to cellular mobile radio – part I: theoretical considerations," IEEE Trans. Commun., vol COM-40(5), pp. 885-894, May 1992.

[53] A. Wittneben, "A new bandwidth efficient transmit antenna modulation diversity scheme for linear digital modulation" in Proc. IEEE ICC'93, vol. 3, pp. 1630-1634, 1993.

[54] J. H. Winters, "On the capacity of radio communication systems with diversity in a Rayleigh fading environment," IEEE J. Select. Areas Commun., vol JSAC-5(5), pp. 871-978, June 1987.

[55] G. J. Foschini, "Layered space-time architecture for wireless communication in a fading environment when using multi-element antennas," AT&T Tech. J., vol. 1, Autumn 1996.

[56] G. D. Forney, "The Viterbi algorithm," Proc. IEEE, vol. 61, pp. 268-278, Mar. 1973.

[57] Bauch, G.and Naguib, A.F., "MAP Equalization of space-time coded signals over frequency selective channels," in Wireless Communications and Networking Conference, vol.1, pp. 261 –265, 1999.

Tables Captions

Figures Captions

Table 3.2.1 The Space Time Codes for Encoder

n_T	*Type*	$\mathbf{a}_{1,0}$	$\mathbf{a}_{1,1}$	$\mathbf{a}_{1,2}$	$\mathbf{a}_{2,0}$	$\mathbf{a}_{2,1}$	$\mathbf{a}_{2,2}$
2	EDC	$(1\ \ 2)^T$	$(1\ \ 3)^T$	$(3\ \ 2)^T$	$(2\ \ 0)^T$	$(2\ \ 2)^T$	$(2\ \ 0)^T$
3	EDC	$(1\ \ 2\ \ 1)^T$	$(1\ \ 3\ \ 2)^T$	$(3\ \ 2\ \ 1)^T$	$(2\ \ 0\ \ 2)^T$	$(2\ \ 2\ \ 0)^T$	$(2\ \ 0\ \ 2)^T$
2	RDC	$(0\ \ 2)^T$	$(1\ \ 2)^T$	$(2\ \ 2)^T$	$(2\ \ 0)^T$	$(1\ \ 1)^T$	$(0\ \ 2)^T$
3	RDC	$(0\ \ 0\ \ 2)^T$	$(0\ \ 1\ \ 2)^T$	$(2\ \ 3\ \ 1)^T$	$(2\ \ 0\ \ 0)^T$	$(1\ \ 2\ \ 0)^T$	$(2\ \ 3\ \ 3)^T$

Table 3.4.1. The maximum values of M given (P,V).

M \ V / P	1	2	3	4	5	6	7	8	9
4	2	1	1	N	N	N	N	N	N
8	4	2	1	N	N	N	N	N	N
12	5	2	1	1	1	N	N	N	N
16	8	4	2	2	1	1	1	N	N

Table 3.4.2. Examples of the (P,V,M) codes.

P	V	M	(P,V,M) code
4	1	2	X1={1 1 1 0}, X2={1 0 1 1}
8	1	4	X1={10000010},X2={10110001} X3={11010111},X4={11100100}
12	1	5	X1={1 0 0 0 0 0 0 1 0 0 1 0} X2={1 0 0 1 0 1 0 0 1 1 1 1} X3={1 0 0 1 1 0 1 1 1 0 0 1} X4={1 0 1 0 1 1 0 0 0 0 0 1} X5={1 1 1 1 0 0 0 1 0 1 0 1}
12	2	2	X1={1 1 1 0 1 0 0 0 1 1 1 0} X2={1 1 1 1 0 1 1 0 1 0 0 0}
16	1	8	X1={0000000001010101} X2={0000111101011010} X3={0011001101100110} X4={0011110001101001} X5={0101010100000000} X6={0101101000001111} X7={0110011000110011} X8={0110100100111100}
16	2	4	X1={0 0 0 0 0 0 1 0 0 1 0 0 1 0 0 1} X2={0 0 1 1 0 0 0 1 0 1 1 1 1 0 1 0} X3={0 1 0 1 0 1 1 1 0 0 0 1 1 1 0 0} X4={0 1 1 0 0 1 0 0 0 0 1 0 1 1 1 1}
16	4	2	X1={1 0 0 0 0 0 1 0 0 1 1 1 0 0 1 0} X2={1 0 1 1 0 0 0 1 0 1 0 0 0 0 0 1}

Table 3.4.3. The codes under test in the numerical simulation.

PROPOSED CODE	x1={1 -1 -1 -1 -1 -1 1 -1} x2={1 -1 1 1 -1 -1 -1 1} x3={1 1 -1 1 -1 1 1 1} x4={1 1 1 -1 -1 1 -1 -1}
PRBS	x1={-1 -1 1 -1 1 1 1} x2={1 -1 1 1 1 -1 -1} x3={1 1 1 -1 -1 1 -1}
ARBITRARY	x1={1 -1 1 -1 -1 -1 1 -1} x2={1 -1 1 1 -1 1 -1 1} x3={1 -1 -1 1 -1 1 1 1} x4={1 1 -1 1 -1 1 1 -1}

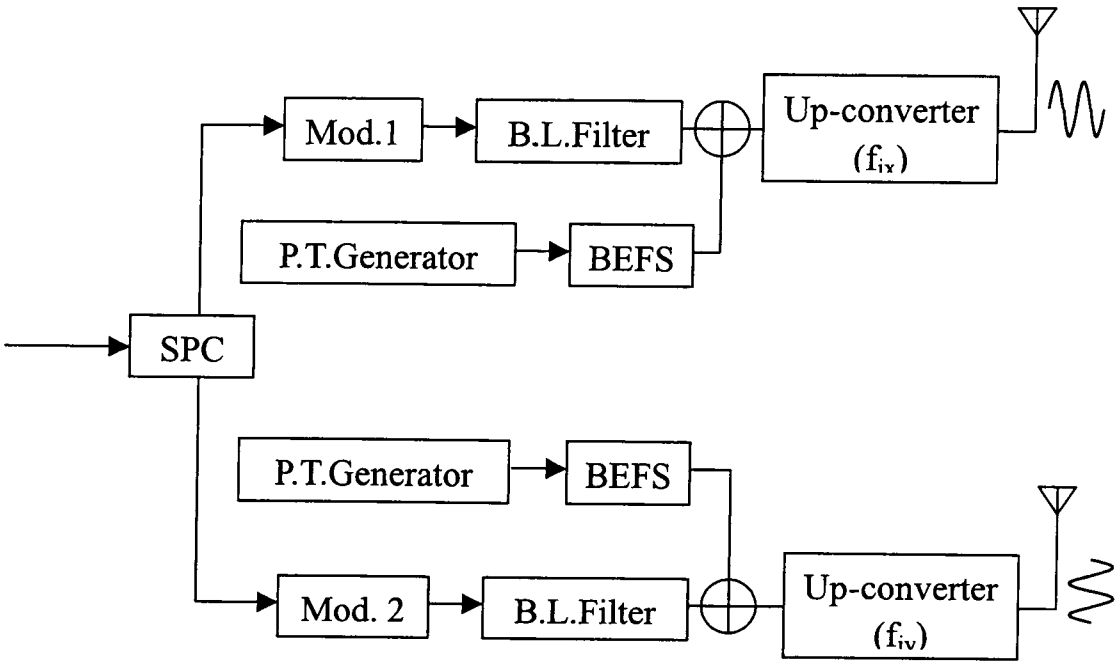

Fig. 3.1.1 The transmitter of the proposed system.

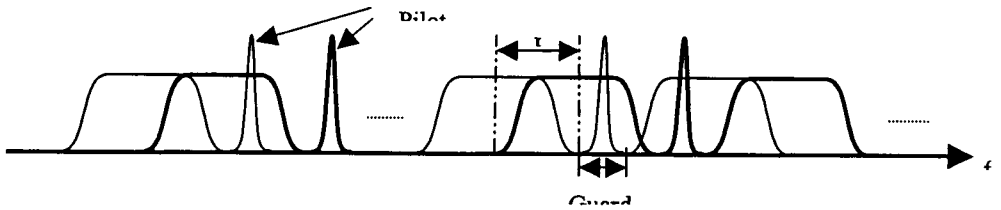

(a) The overall signal spectrum include pilot tones.

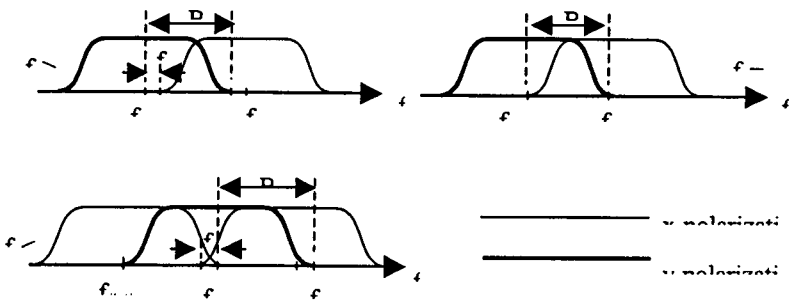

(b) Diagram of CPI due to frequency overlap.

Fig. 3.1.2 Sketch of frequency band allocation and frequency shifting.

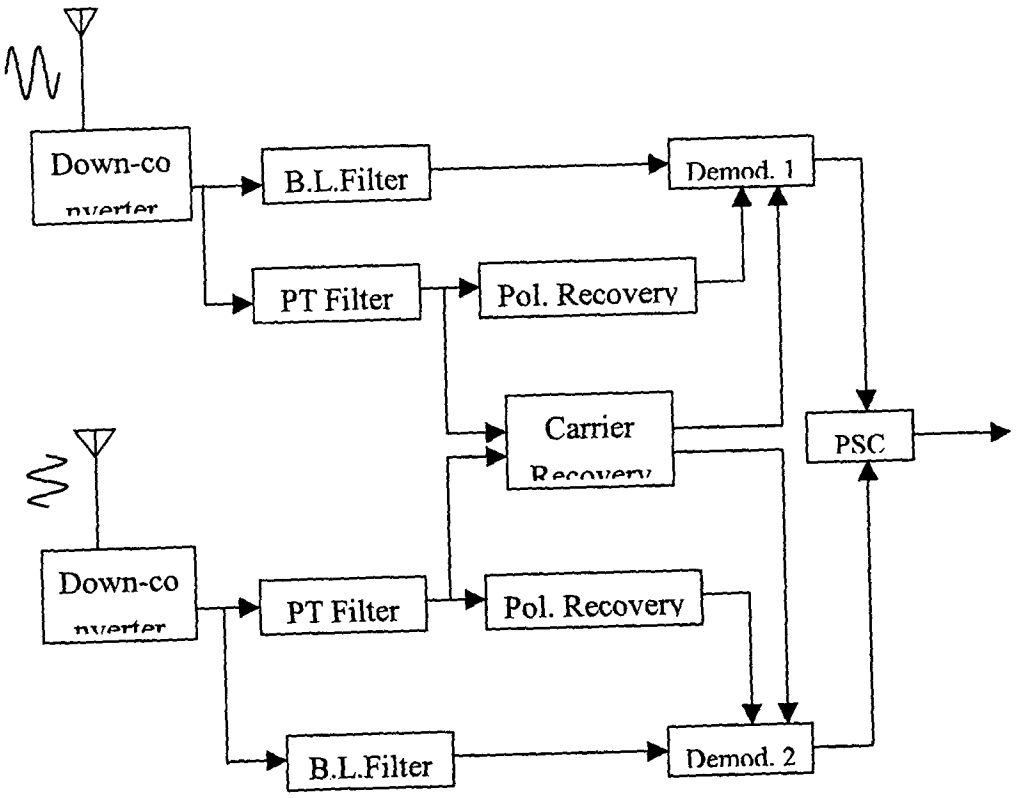

Fig. 3.1.3 The receiver of the proposed system.

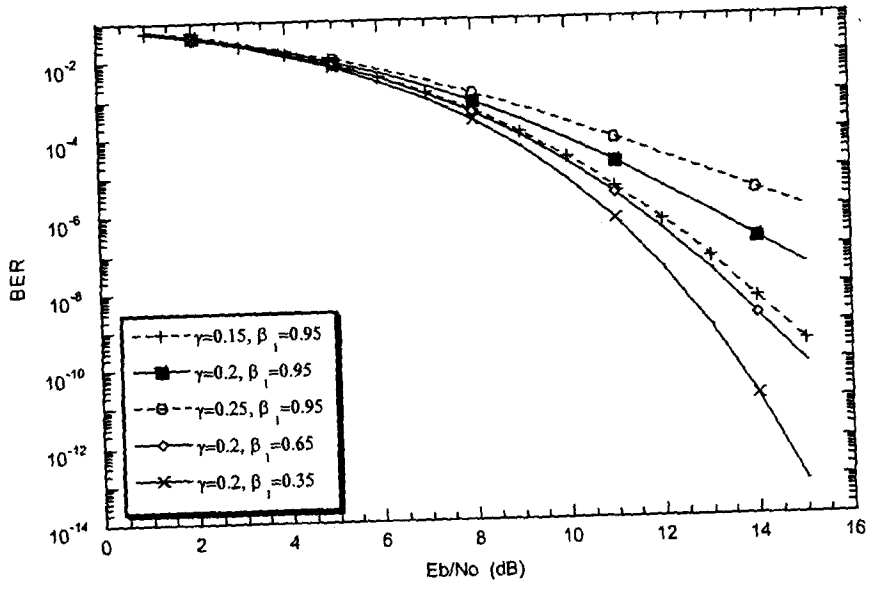

Fig. 3.1.4 Performance with various values of γ and β_1 for Δ_1=0.2, Δ_2=0.3, δ=0.3, R=0.2, β=0, Δ=0.2, β_1=0.95.

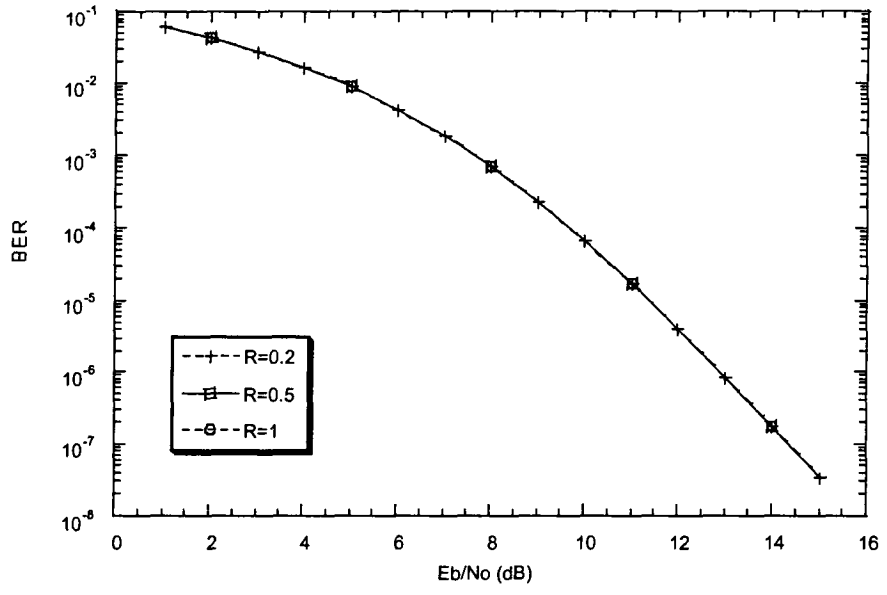

Fig. 3.1.5 Performance with various values of R for Δ_1=0.2, Δ_2=0.3, δ=0.3, γ=0.2, β=0,

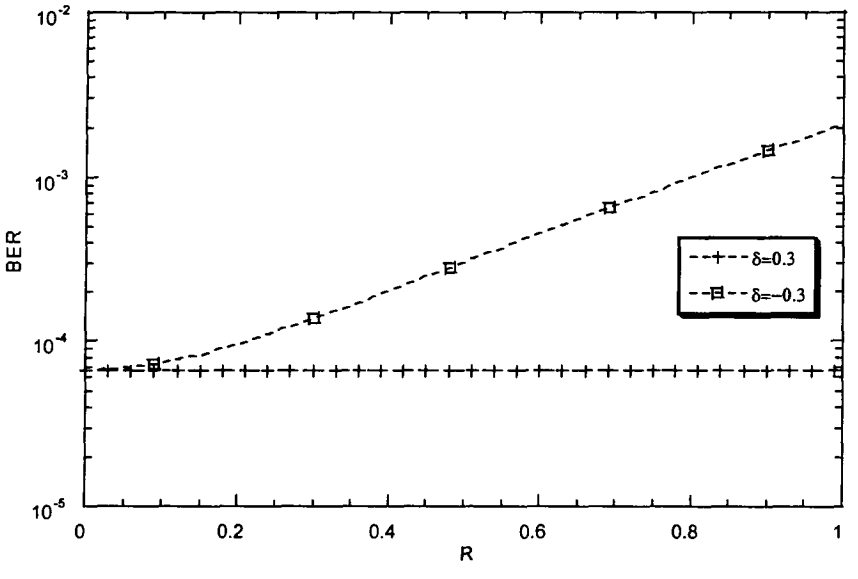

Fig. 3.1.6 Performance versus R with various values of δ for Δ_1=0.2, Δ_2=0.3, γ=0.2, β=0, Δ=0.2, β_1=0.95, Eb/N0=10 (dB).

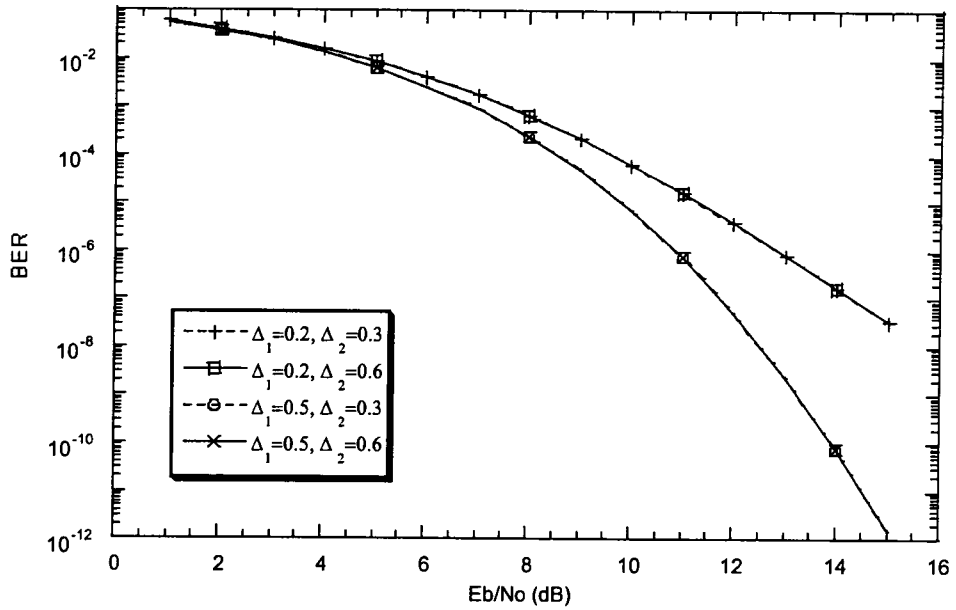

Fig. 3.1.7 Performance with various values of Δ_1 and Δ_2 for γ=0.2, δ=0.3, R=0.2, β=0, Δ=0.2, β_1=0.95.

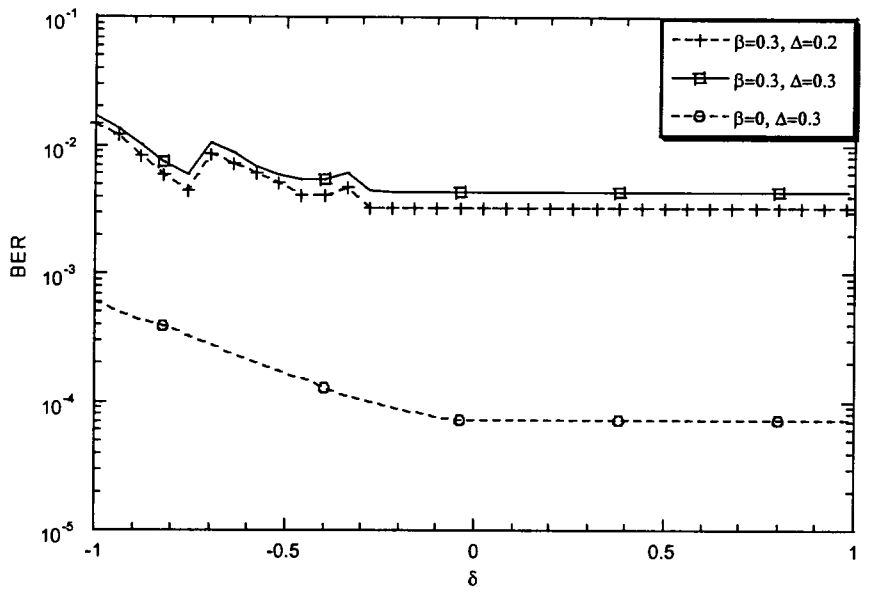

Fig. 3.1.8 Performance versus δ with various values of β and Δ for Δ_1=0.2, Δ_2=0.3, γ=0.2, R=0.2, β_1=0.95, Eb/No=10 (dB).

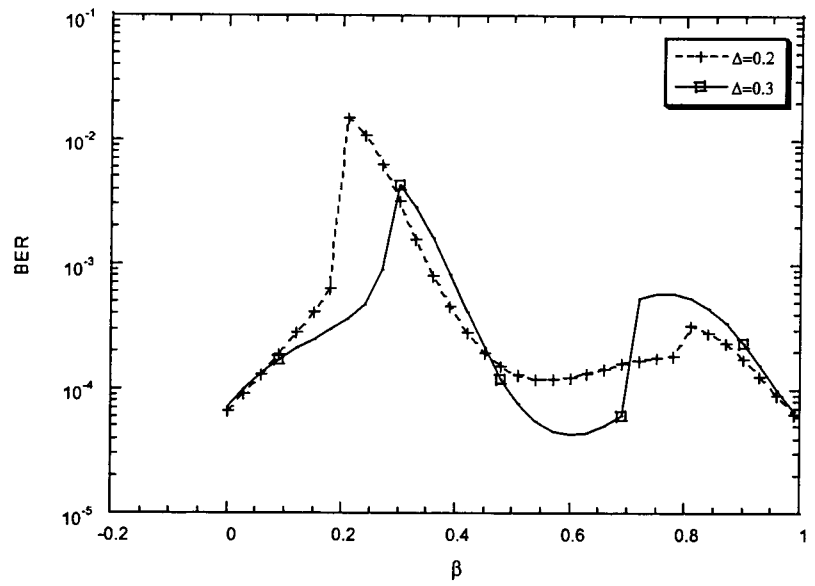

Fig. 3.1.9 Performance versus β with various values of Δ for Δ_1=0.2, Δ_2=0.3, δ=0.3, γ=0.2, R=0.2, β_1=0.95, Eb/No=10 (dB).

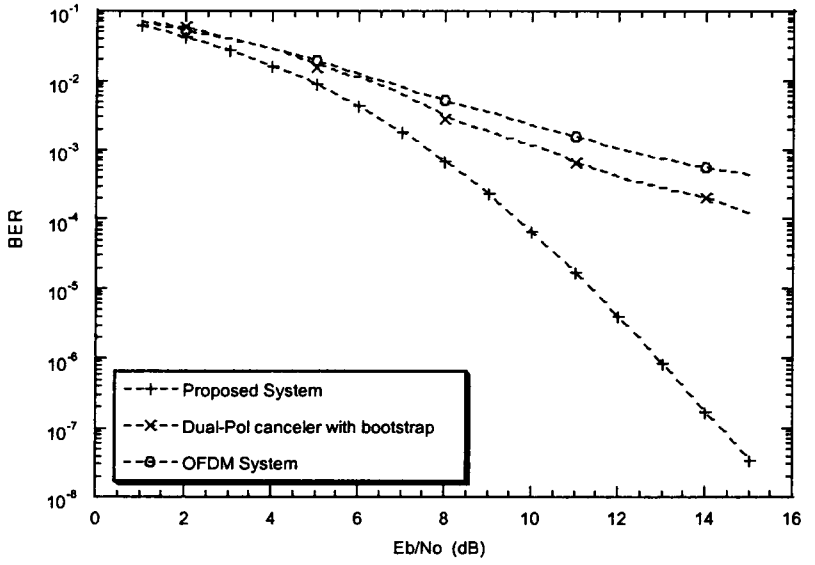

Fig. 3.1.10 Performance comparison with the dual-polarization. cancellation system and the OFDM system.

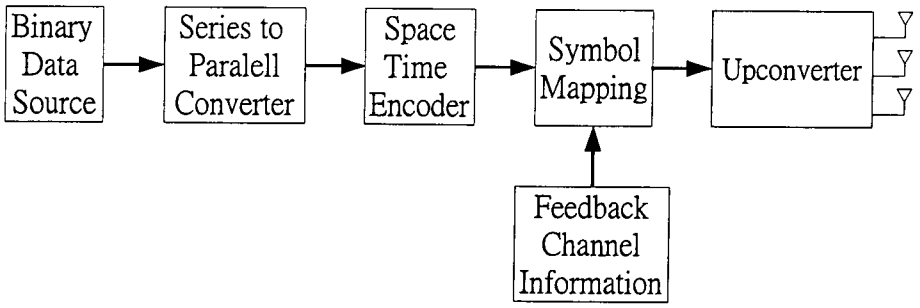

(a)

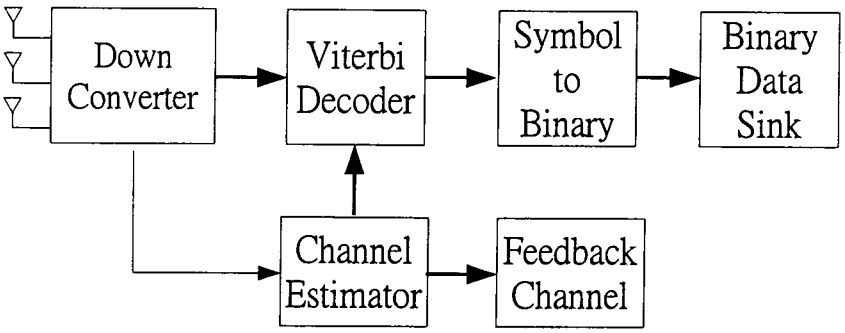

(b)

Fig. 3.2.1 (a) The Transmitter Block Diagram (b) The Receiver Block Diagram

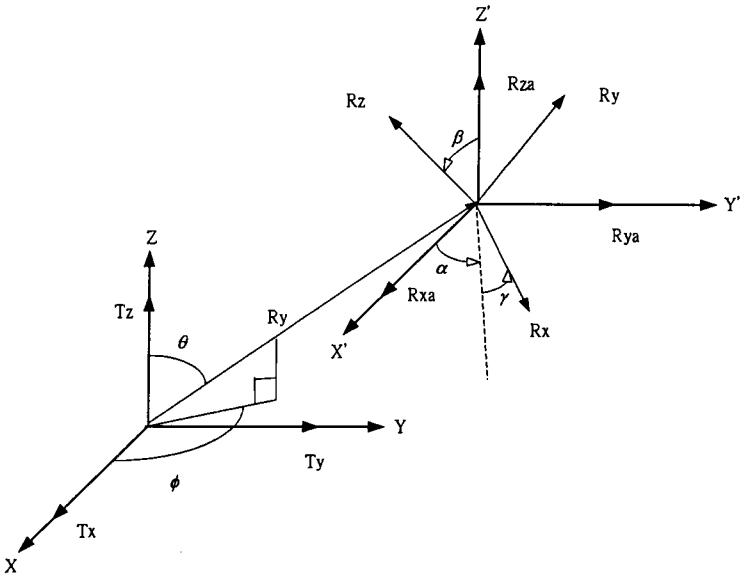

(a)

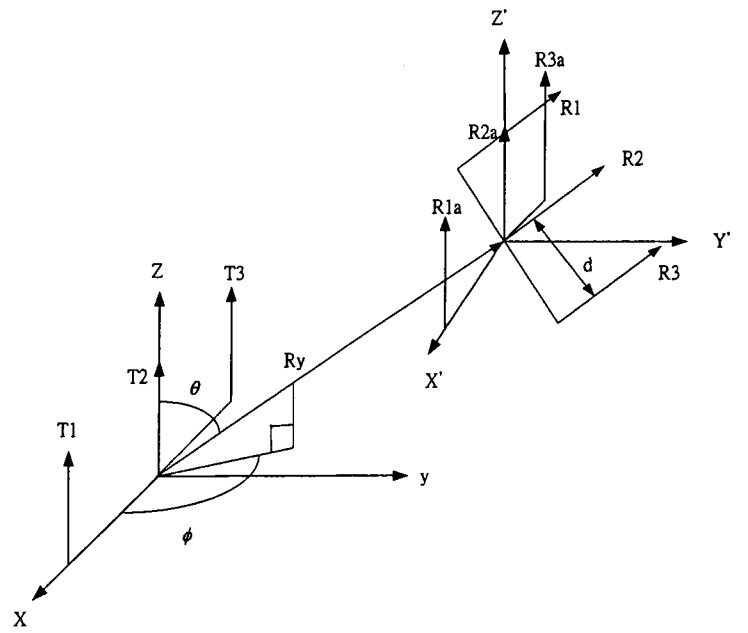

(b)

Fig. 3.2.2 The relative locations and orientations of the transmitter and the receiver with (a) orthogonal antenna sets (b) collinear antenna sets

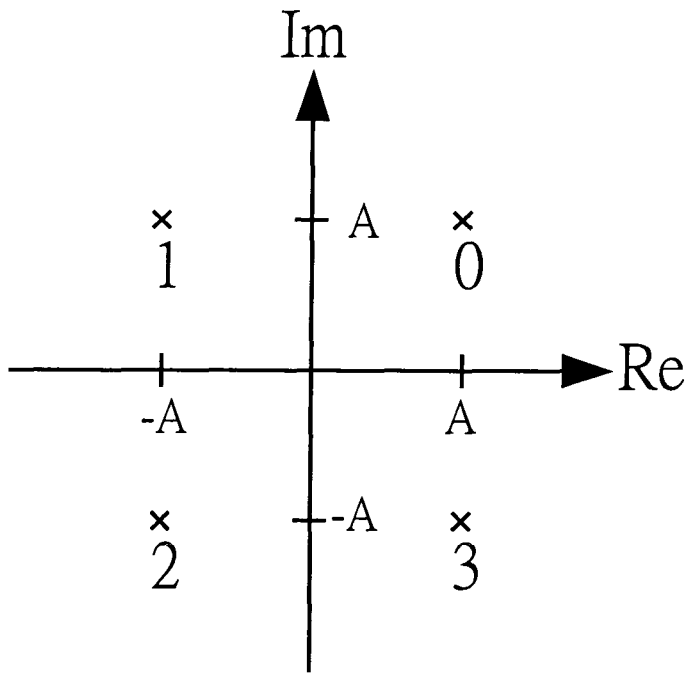

Fig. 3.2.3 The symbol constellations

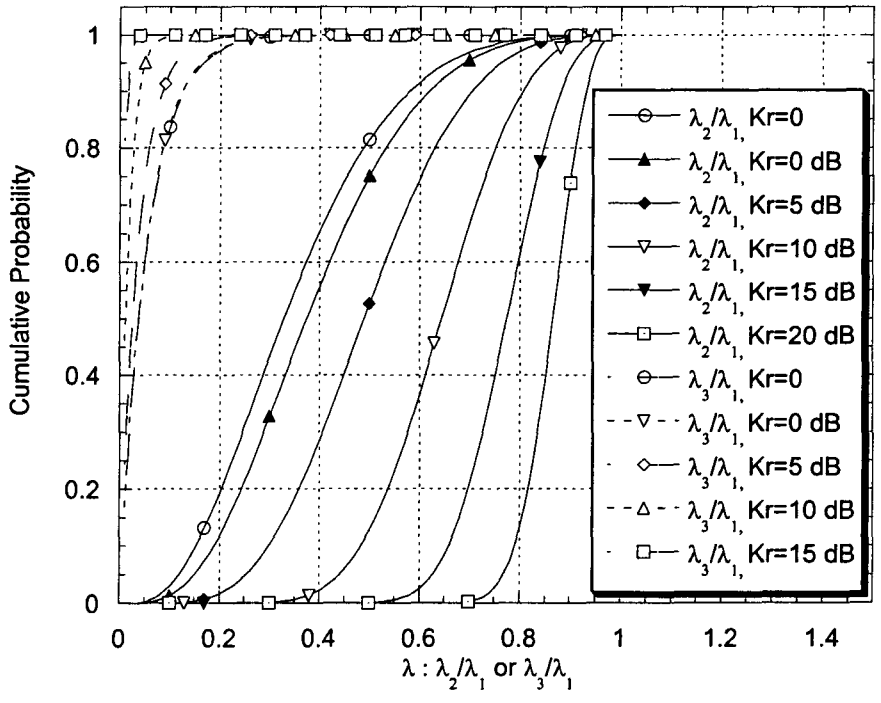

Fig. 3.2.4 The cumulative probability of the relative value of eigenvalues

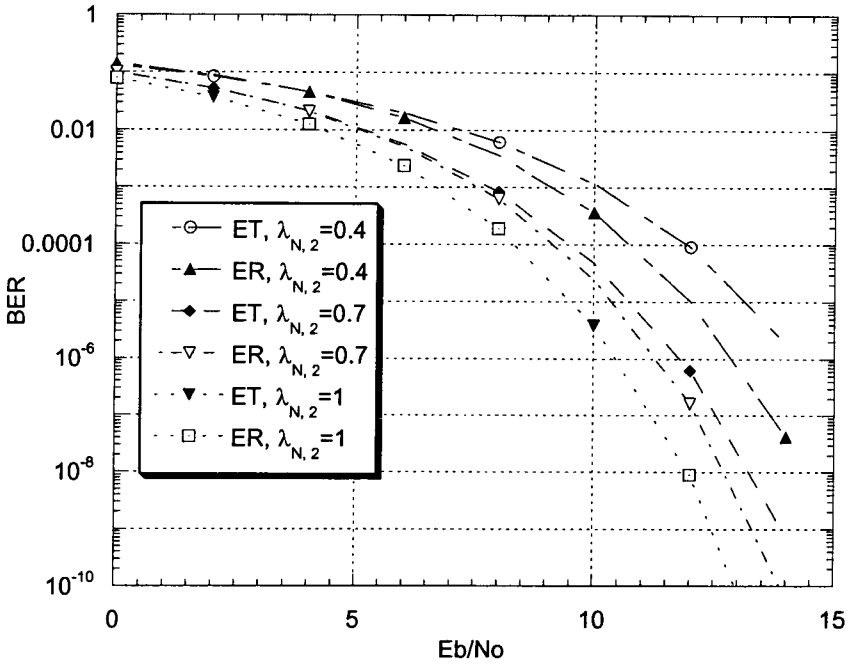

Fig. 3.2.5 Comparison of average uncoded bit error probability between E-T and E-R constellations

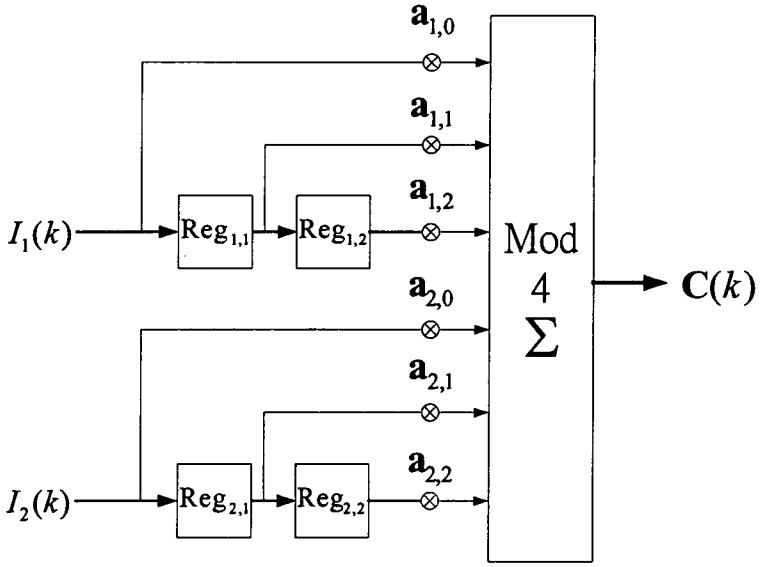

Fig. 3.2.6 The Space Time Encoder

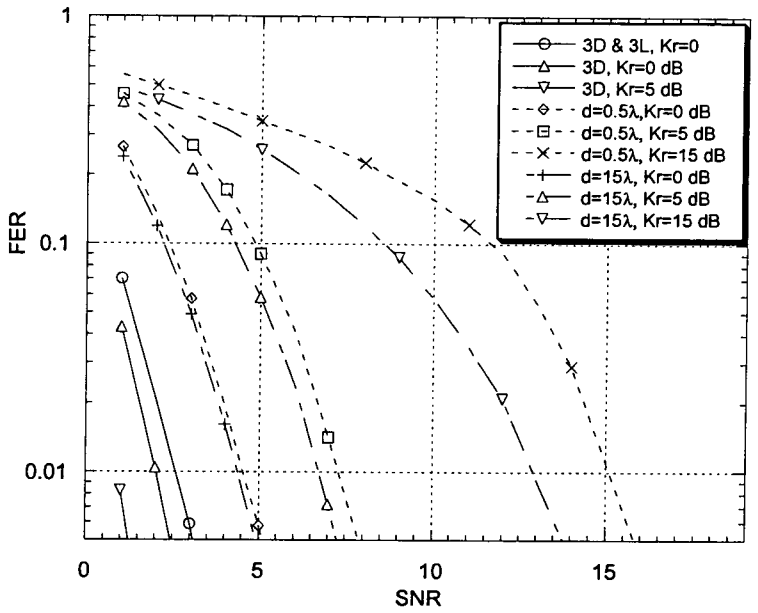

Fig.3.2.7 Outage Probability for 3-D antenna set and 3-L antenna set

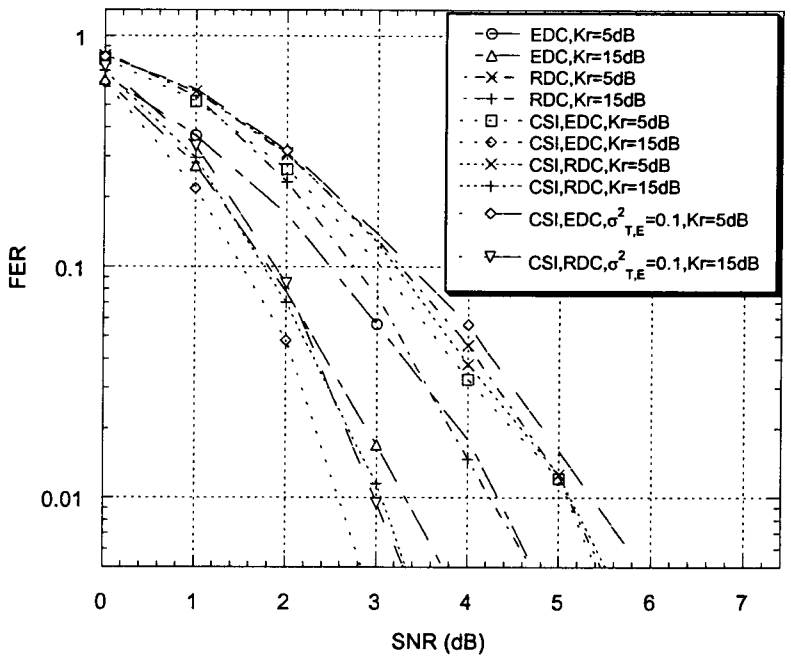

Fig. 3.2.8 Frame error probability of EDC and RDC space-time codes

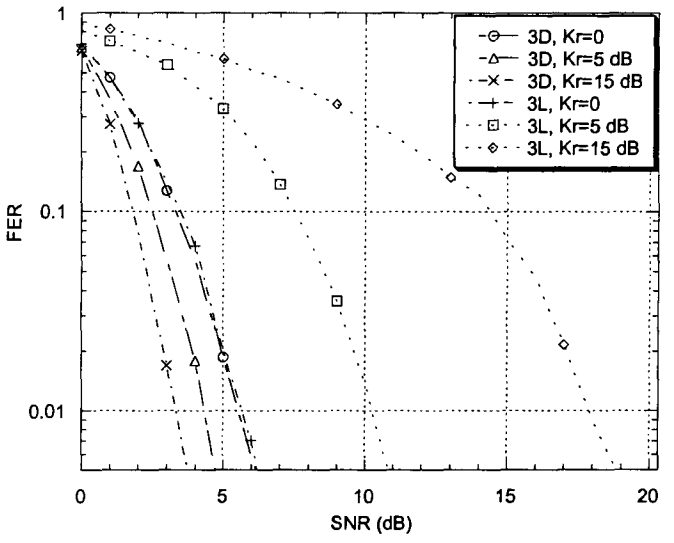

Fig. 3.2.9 Frame error probability of 3D and 3L antenna sets with EDC space-time code

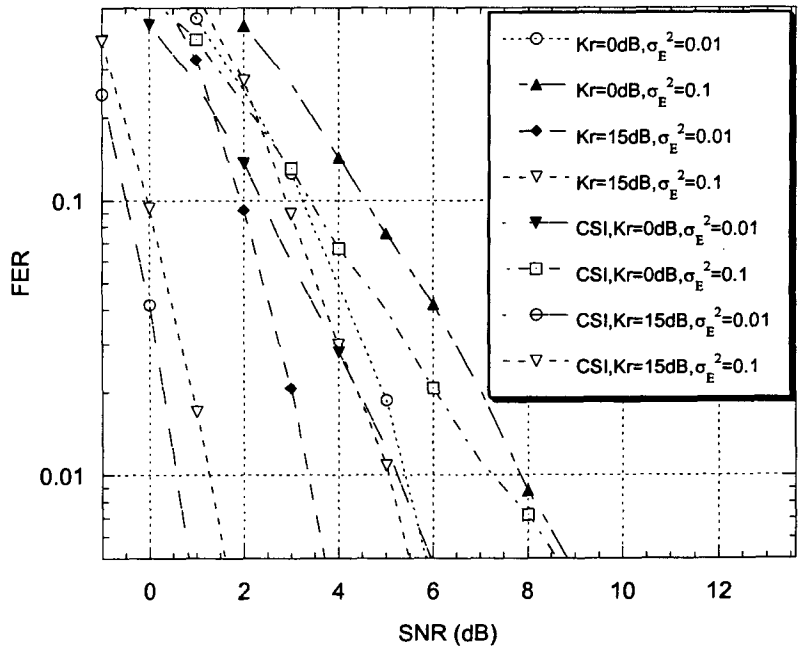

Fig. 3.2.10 System performance with imperfect channel estimation

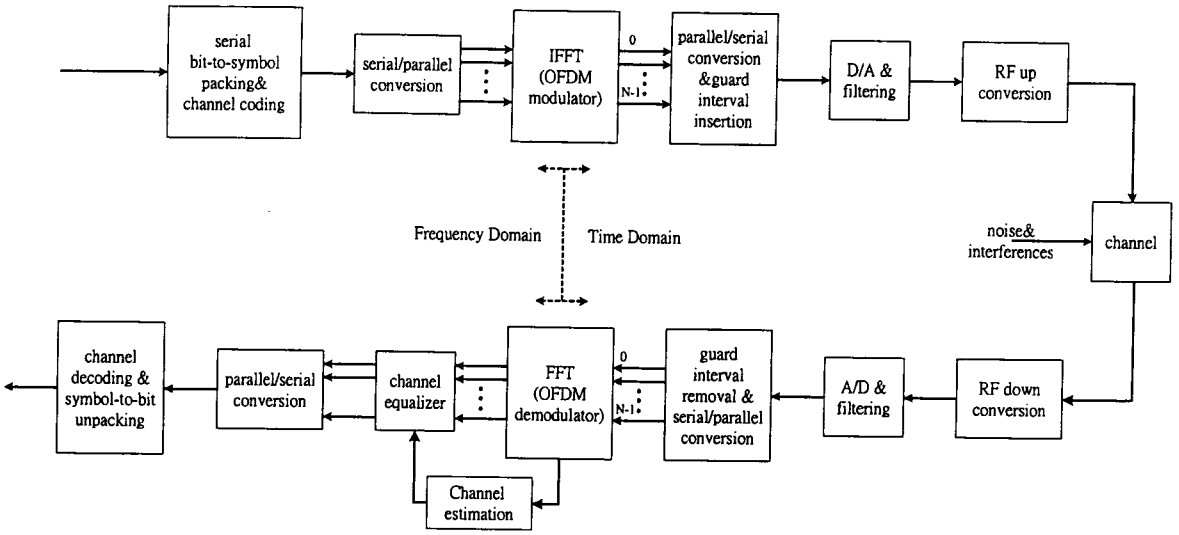

Fig. 3.3.1. The OFDM system block.

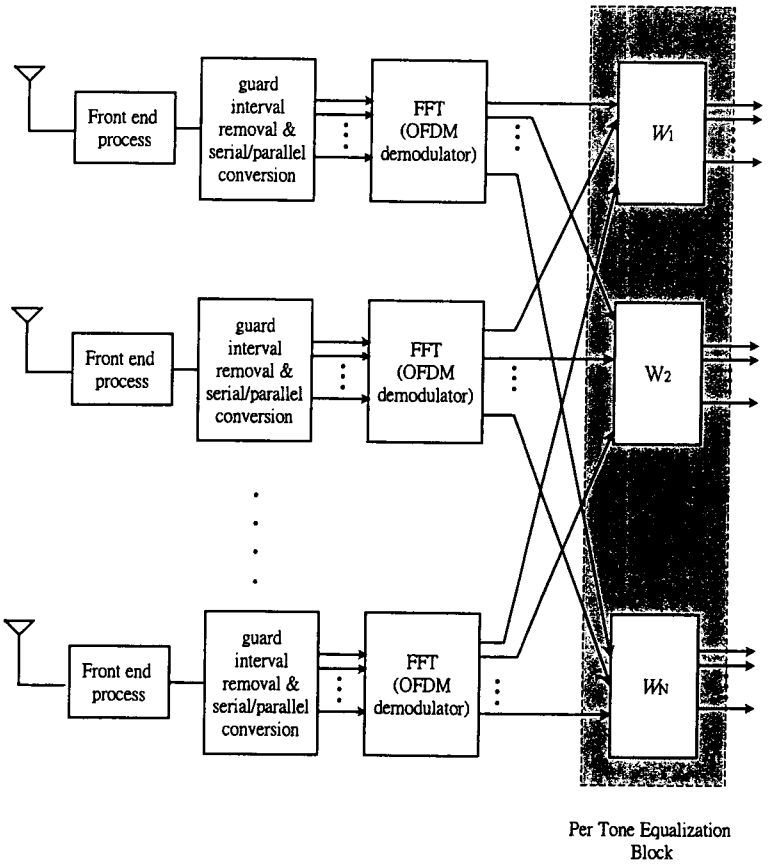

Fig. 3.3.2. The Receiver structure.

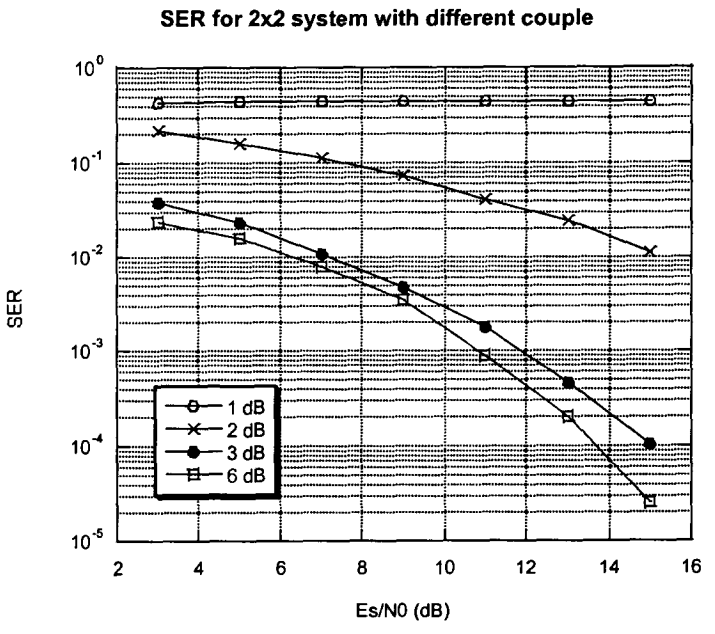

Fig. 3.3.3. Symbol error rate for two-input two-output system with MMSE equalization for various power coupling coefficient.

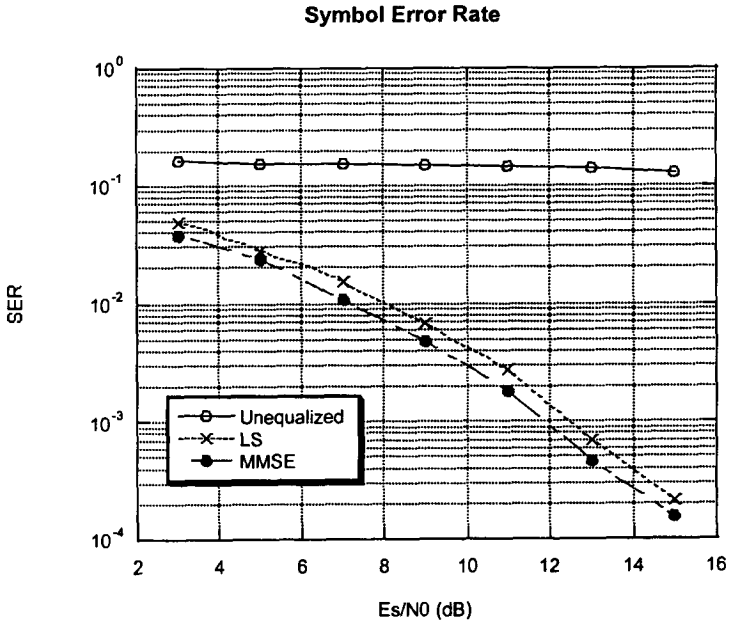

Fig. 3.3.4. Symbol error rates of the two-input two-output OFDM system with 3 dB coupling and various equalizers

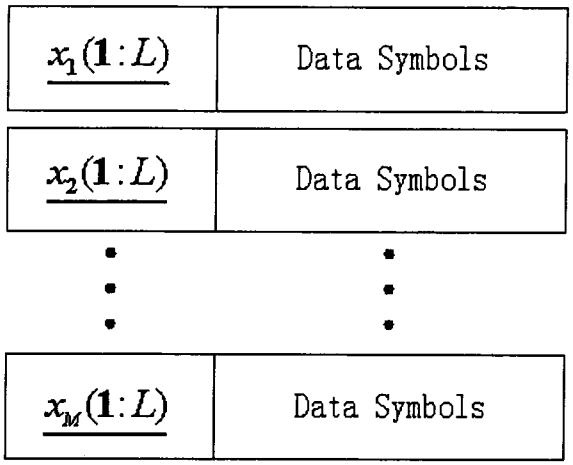

Fig.3.4.1 The burst data structure for M -antenna transmission

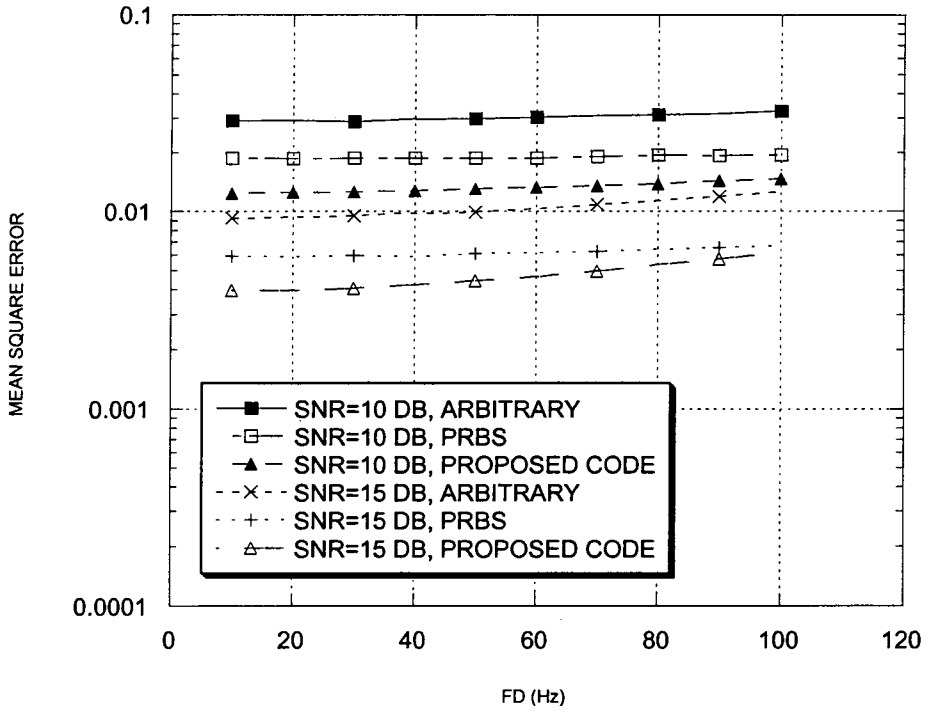

Fig. 3.4.2. Performance Comparison of three sequence sets with Doppler frequency shift.

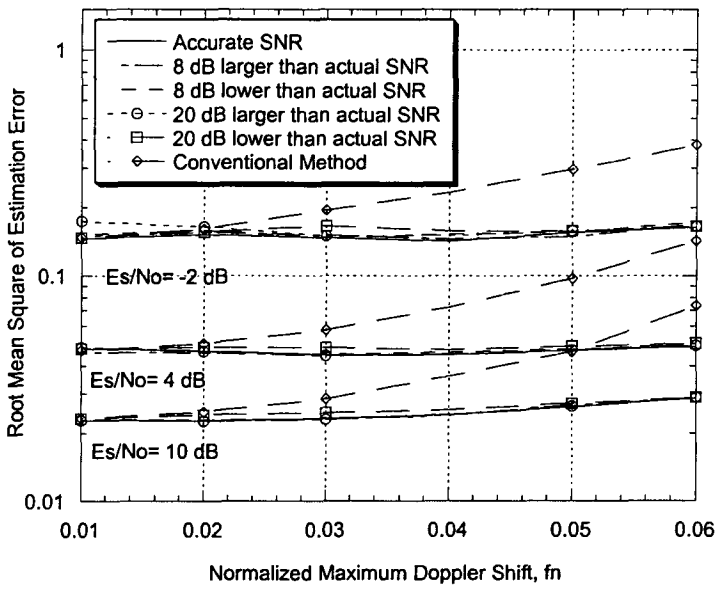

Fig 3.5.1. Performance comparison with the conventional scheme for various inaccurate SNR values

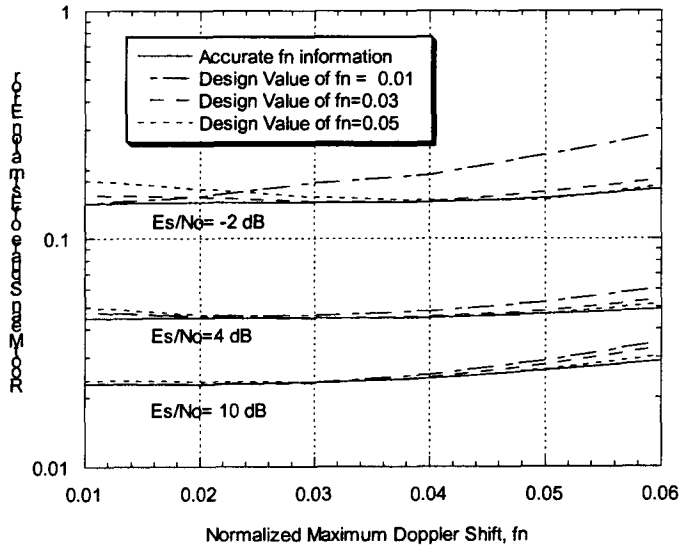

Fig 3.5.2. Performance for various designed value of f_n

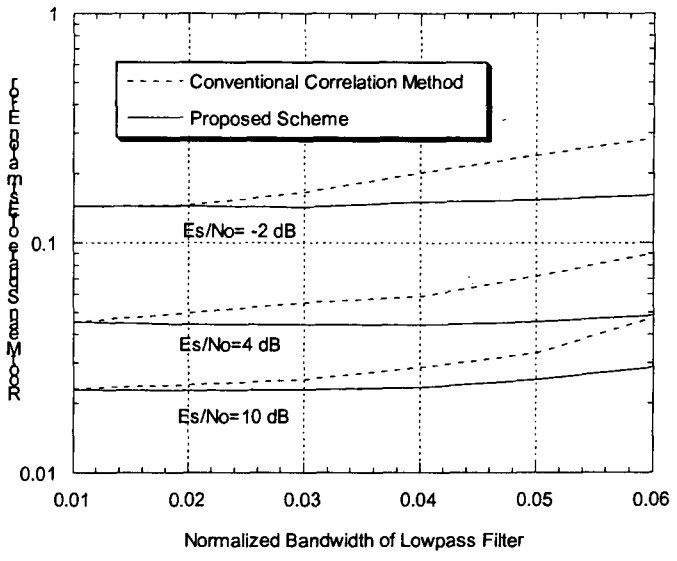

Fig. 3.5.3 Performance Comparison with Channel Model Mismatch

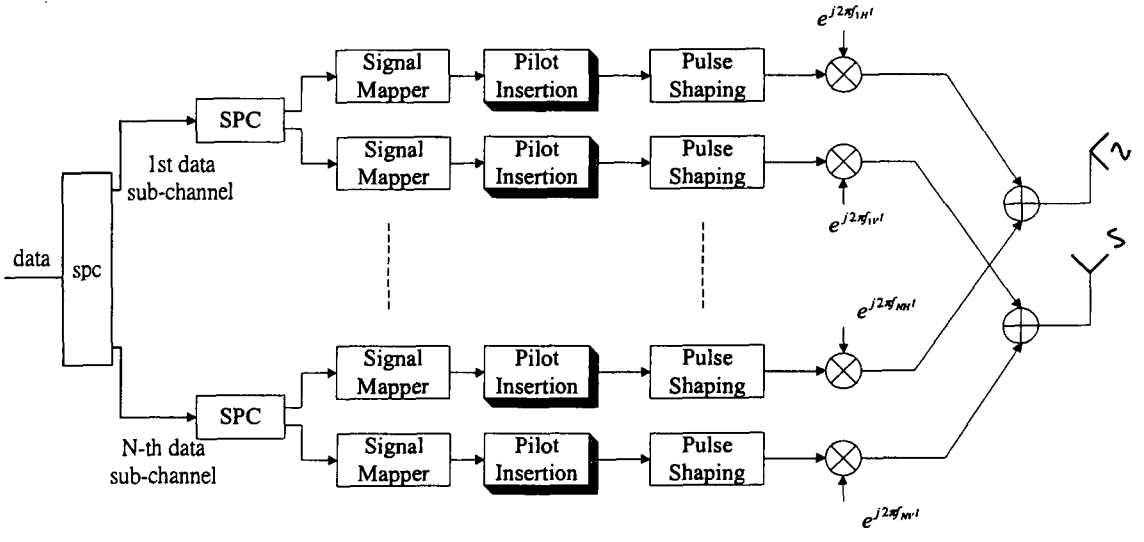

Fig. 3.6.1 The transmitter structure of the proposed system

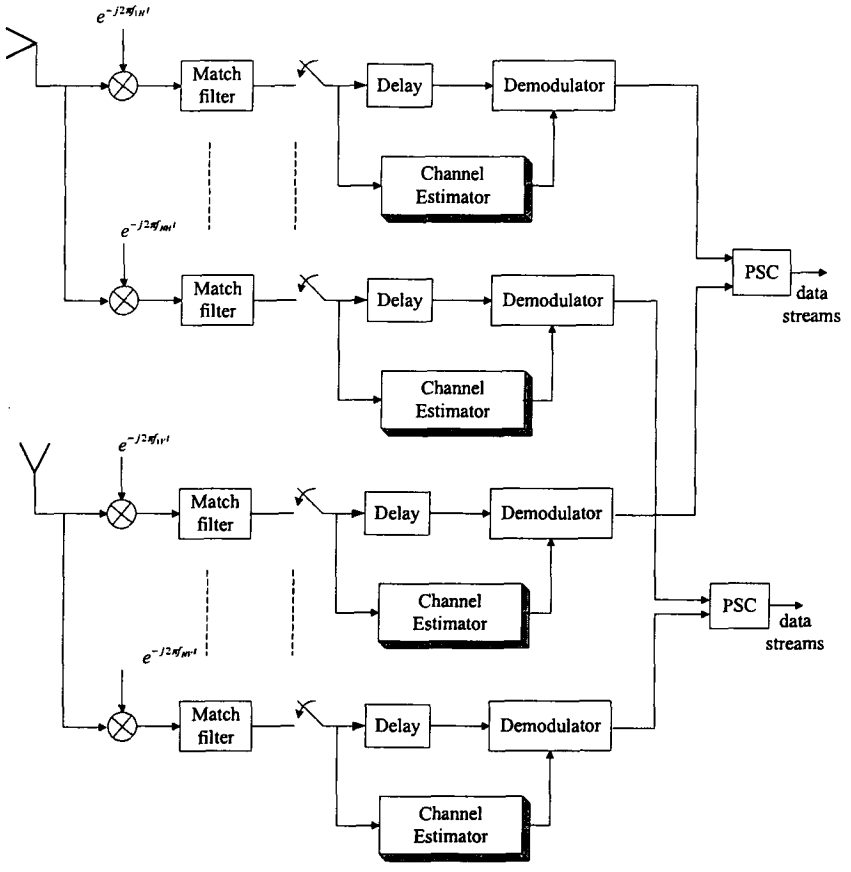

Fig. 3.6.2 The receiver structure of the proposed system

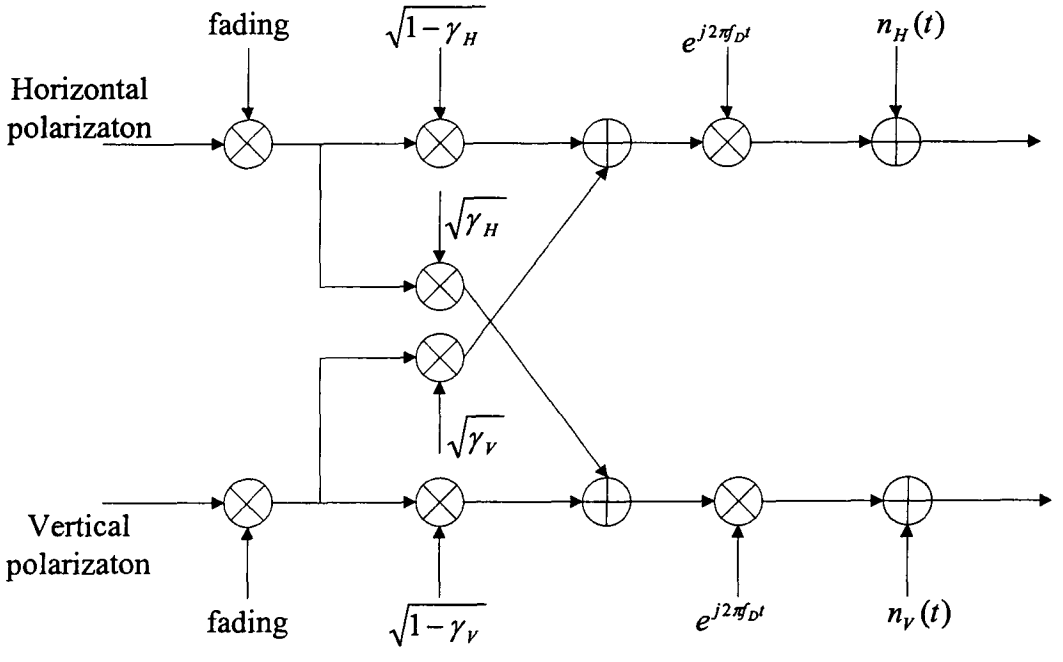

Fig. 3.6.3 The channel model of the proposed system

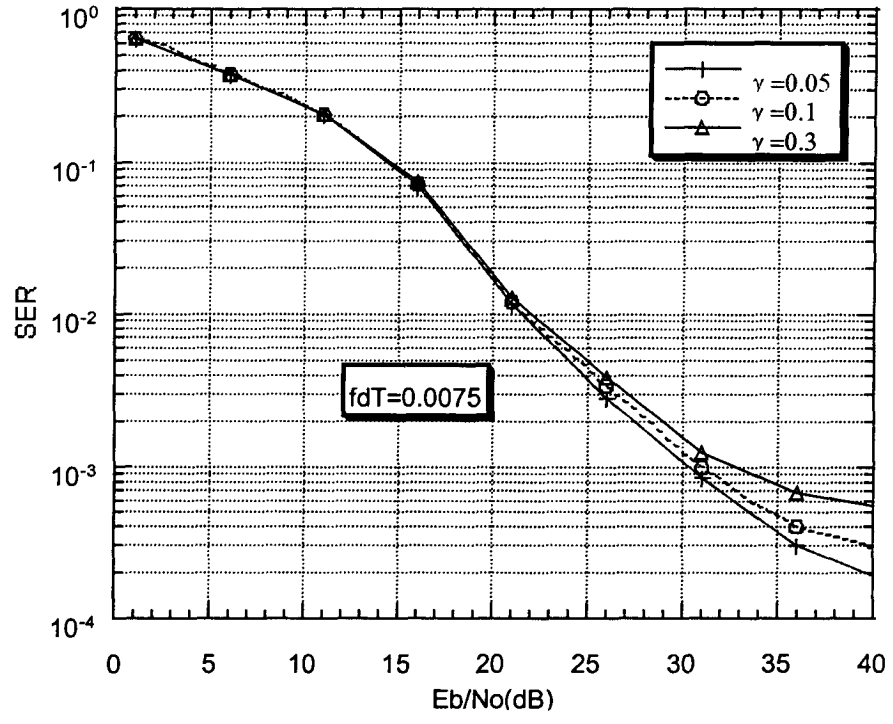

Fig. 3.6.4 The system performance for various values of the power coupling

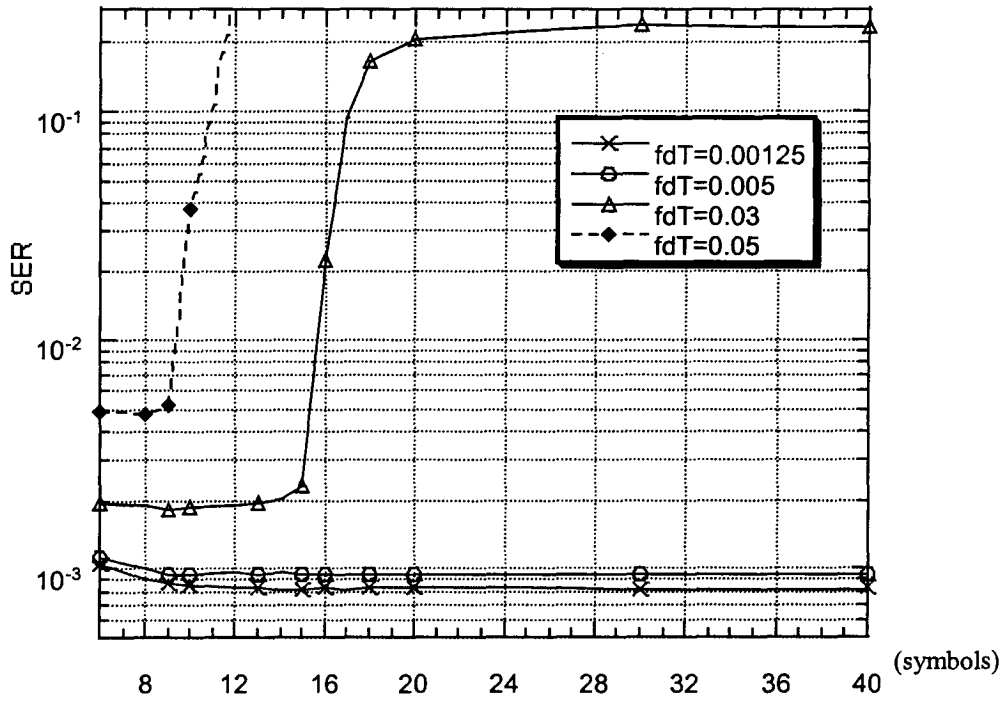

Fig. 3.6.5 The effect due to the pilot spacing on the system performance

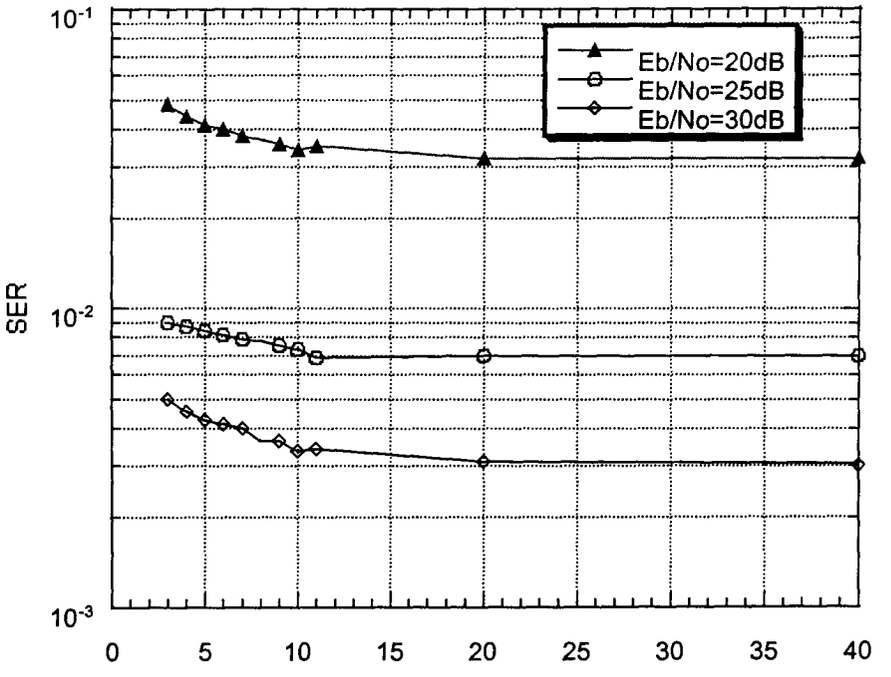

Fig. 3.6.6 The system performance versus the interpolation size

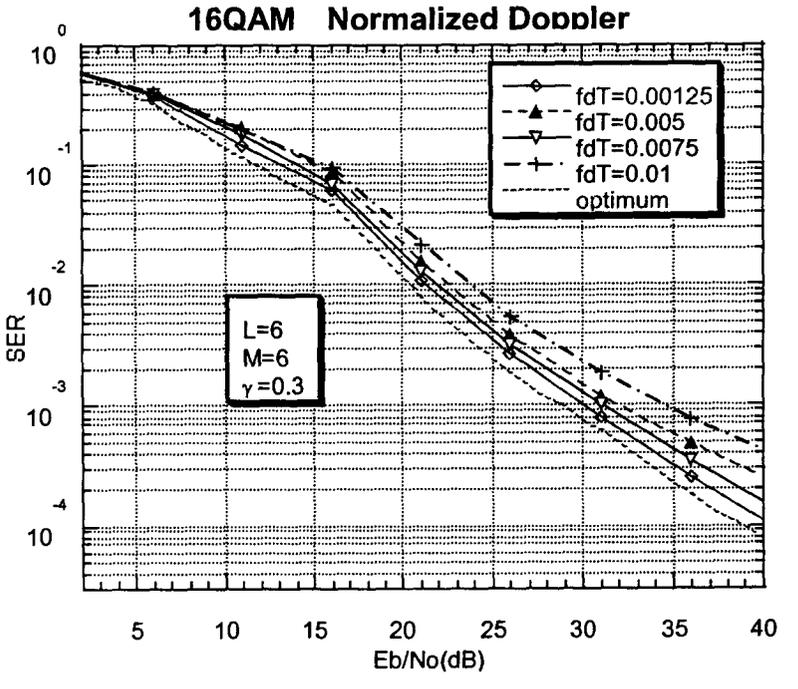

Fig. 3.6.7 The system performance with various value of normalized Doppler spread

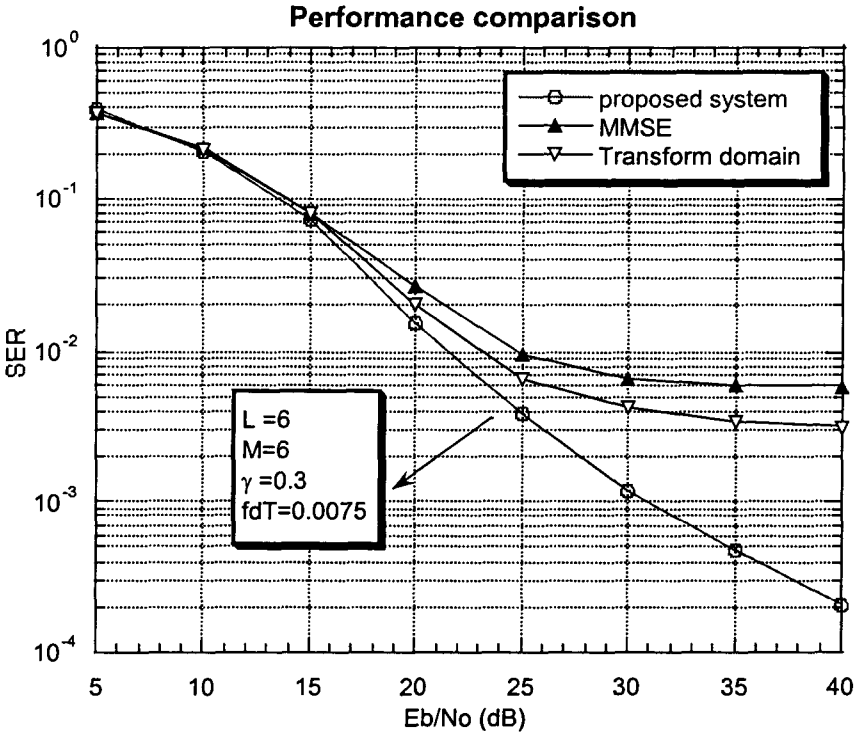

Fig. 3.6.8 Performance comparison of the proposed system and the systems with MMSE estimate and linear interpolation in transform domain

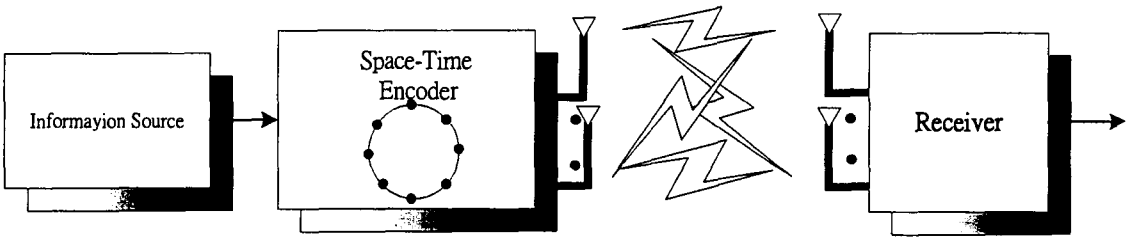

Fig. 3.7.1: Transmit Diversity with Space-Time Coding

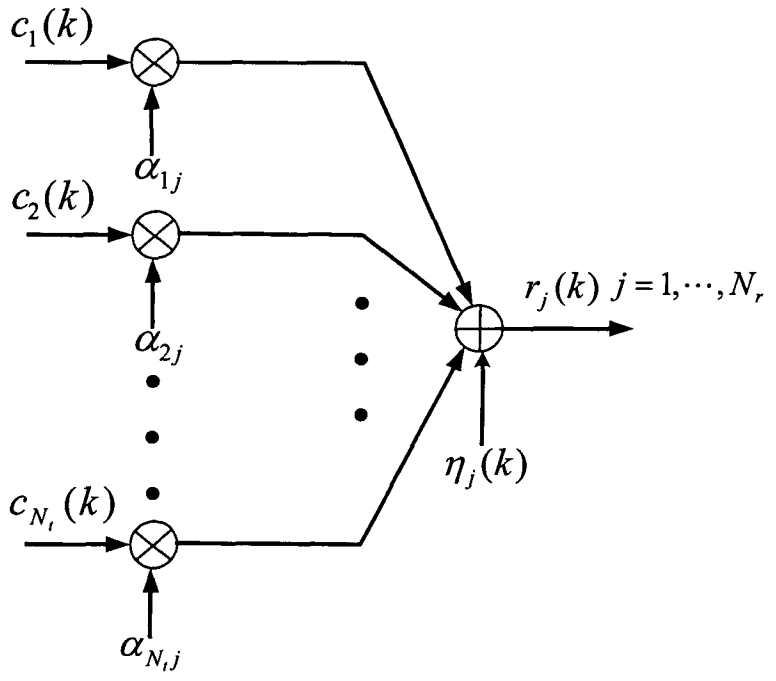

Fig. 3.7.2: Equivalent System Model of MC-MLSE with Transmit Diversity per basis of the Receive Antenna

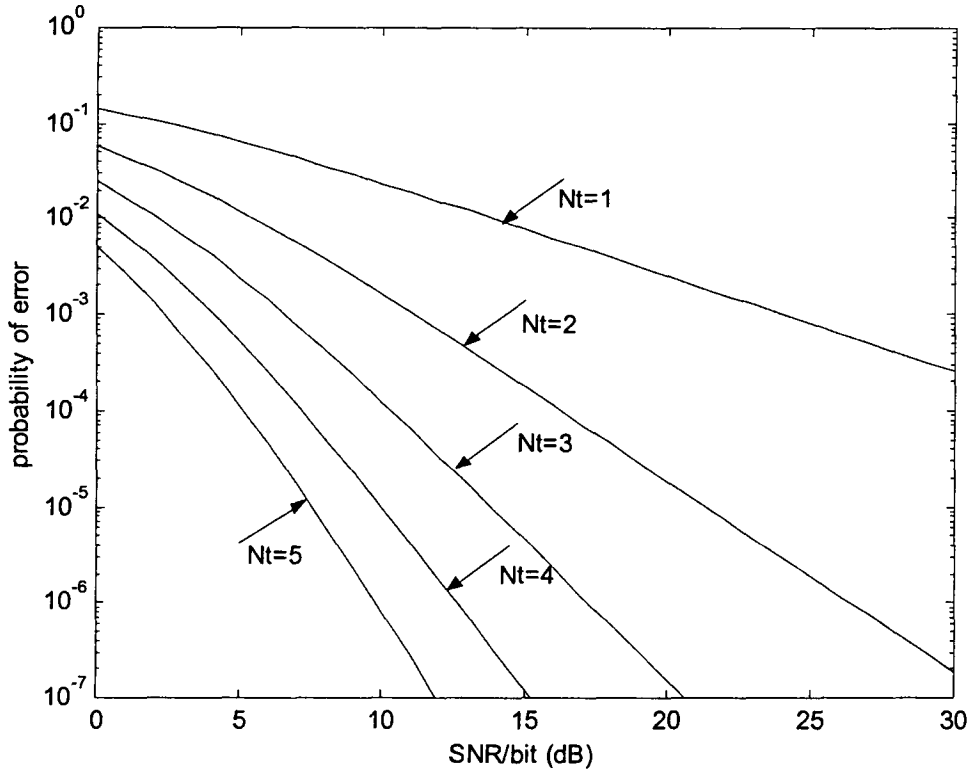

Fig. 3.7.3 Theoretical MFB on MC-MLSE with Transmit Diversity N_t

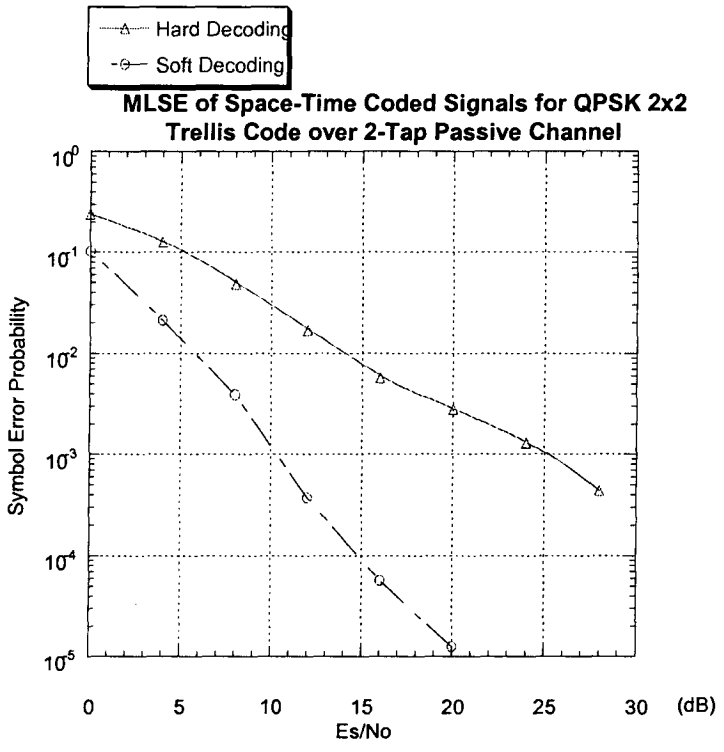

Fig. 3.7.4 Performance of MC-MLSE Equalizer of Space-Time Coded Signals for Both Soft and Hard Decoding

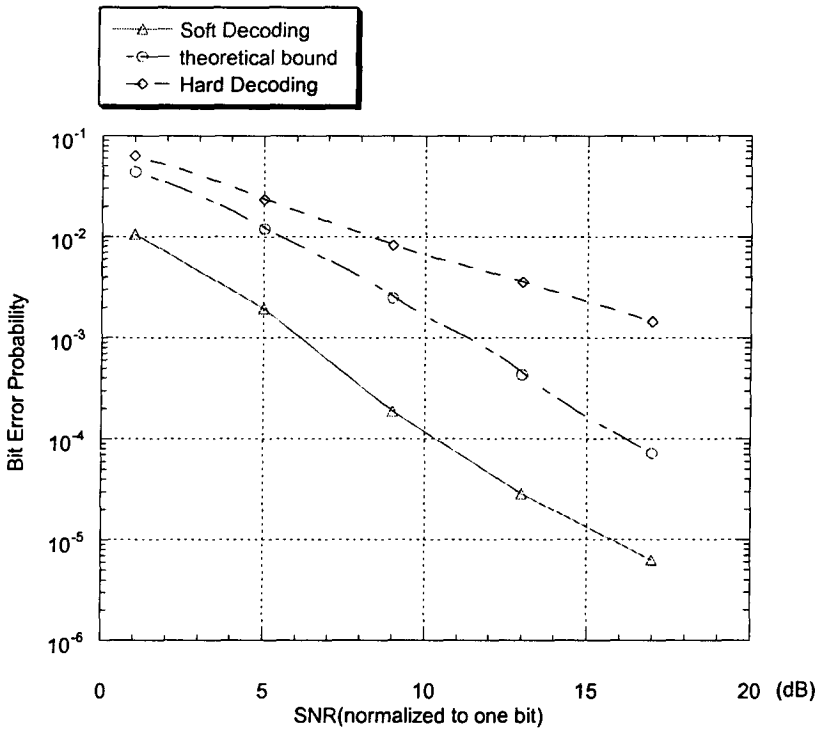

Fig. 3.7.5 Performance Comparison with respect to Theoretical Bound

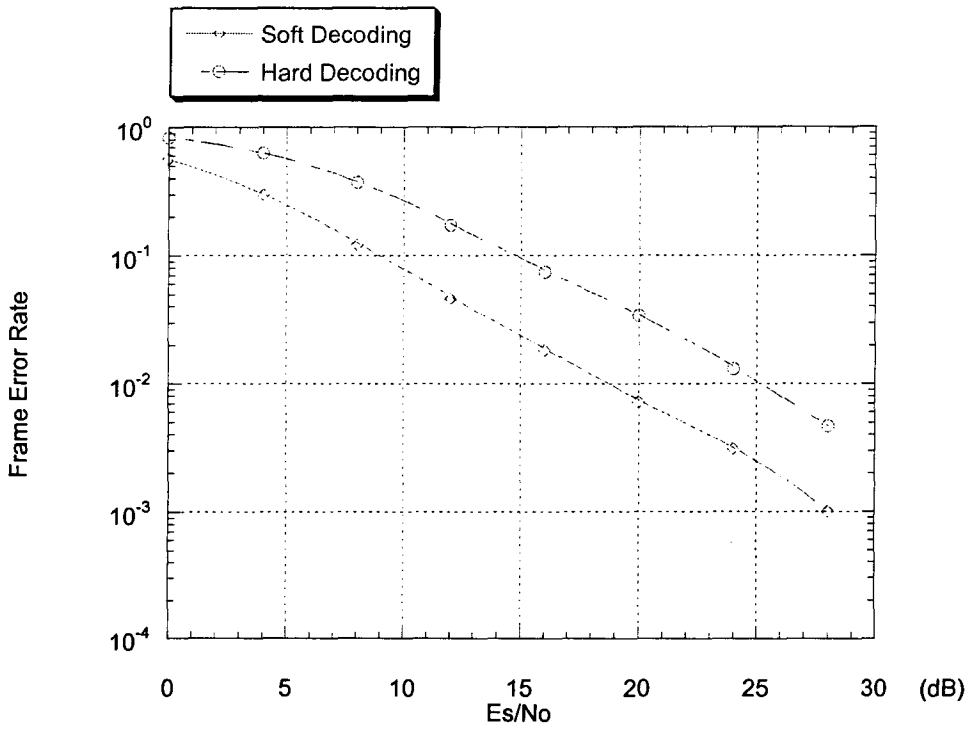

Fig. 3.7.6 Frame Error Rate of Space-Time Coded Transmission with MC-MLSE for Both Soft and Hard Decoding